Chemosensors **2015**, *3*, 70-117; doi:10.3390/chemosensors3020070

OPEN ACCESS

chemosensors

ISSN 2227-9040

www.mdpi.com/journal/chemosensors

Review

X-Ray Photoelectron Spectroscopic Characterization of Chemically Modified Electrodes Used as Chemical Sensors and Biosensors: A Review

Elio Desimoni [†,*] **and Barbara Brunetti** [†]

DeFENS, University of Milan, via Celoria 2, Milan (I) 20133, Italy;
E-Mail: barbara.brunetti@unimi.it

† These authors contributed equally to this work.

* Author to whom correspondence should be addressed; E-Mail: elio.desimoni@unimi.it;
Tel.: +39-025-031-9223; Fax: +39-025-031-9227.

Academic Editors: Michael Ongaro and Paolo Ugo

Received: 3 December 2014 / Accepted: 27 March 2015 / Published: 10 April 2015

Abstract: The characterization of chemically modified sensors and biosensors is commonly performed by cyclic voltammetry and electron microscopies, which allow verifying electrode mechanisms and surface morphologies. Among other techniques, X-ray photoelectron spectroscopy (XPS) plays a unique role in giving access to qualitative, quantitative/semi-quantitative and speciation information concerning the sensor surface. Nevertheless, XPS remains rather underused in this field. The aim of this paper is to review selected articles which evidence the useful performances of XPS in characterizing the top surface layers of chemically modified sensors and biosensors. A concise introduction to X-ray Photoelectron Spectroscopy gives to the reader the essential background. The application of XPS for characterizing sensors suitable for food and environmental analysis is highlighted.

Keywords: chemically modified sensors; biosensors; X-ray photoelectron spectroscopy; surface analysis of electrodes; electrocatalysis

1. Introduction

According to IUPAC, chemically modified electrodes (CMEs) are electrodes made of a conducting or semiconducting material that is coated with a selected monomolecular, multimolecular, ionic, or polymeric film of a chemical modifier and that, by means of faradaic (charge-transfer) reactions or interfacial potential differences (no net charge transfer), exhibit chemical, electrochemical, and/or optical properties of the film [1]. Applications of CMEs span from solar energy conversion and storage, to batteries, selective electro-organic synthesis, molecular electronics, electrochromic display devices, corrosion protection, electrocatalysis and food or environmental analyses.

CMEs suitable as chemical sensors and biosensors (both named "sensors" from now on) have been reviewed in a large series of papers describing their exciting performances. See references [2–15] for some recent examples.

Investigations aimed at developing new sensors and evaluating their performances usually employ combined experimental techniques. Cyclic voltammetry (CV) and electron microscopies are those most generally used, since they allow a main access to electrode micro-mechanisms and surface morphologies. Other techniques are more and more exploited for improving the characterization of surface films, such as Atomic Force Microscopy (AFM), Fourier Transform Infrared (FTIR), Electrochemical Impedance Spectroscopy (EIS), X-ray Diffraction (XRD), Scanning Electrochemical Microscopy (SECM), X-ray Photoelectron Spectroscopy (XPS) and others (all acronyms used in this review are also expanded in the Appendix). In particular, XPS (in the past also known as ESCA-Electron Spectroscopy for Chemical Analysis) allows acquiring otherwise inaccessible information about the qualitative, quantitative (or at-least semi-quantitative) and, most of all, speciation status of the CME surface. However, XPS remains rather underused in this field. The literature information considered here below spans from 2010 to about mid 2014. Inevitably, taking into account the huge number of relevant articles, this review is not exhaustive. For this period, Scopus returns 4826 documents relevant to "modified electrodes", restricted to "only" 157 (about the 3%) if the search is extended to "modified electrodes" and "ESCA" or "XPS".

After an as much as possible concise introduction to XPS, in order to give the reader the essential background, the attention focuses to those papers, arbitrarily selected within those above-mentioned, in which XPS findings give a significant contribution to a better sensor characterization. To limit the length of the review, the analytical performances of the sensors (linear ranges, limits of detection, selectivity, repeatability *etc.*), as claimed by the various authors, are not considered here below. Sensor architectures are represented by using the format *surface layer/eventual middle layers/electrode material*.

2. An Introduction to Photoelectron Spectroscopy

Several qualified books and reviews (see for example [16–22]) present principles and practices of XPS. Nevertheless, the very basic principles of the technique are detailed below for allowing the inexperienced reader a reasonable understanding of the reviewed results.

In XPS, a solid sample is introduced in a chamber maintained under ultra-high vacuum (UHV, below 10^{-8} mbar) where it is irradiated with soft X-rays, usually with Mg Kα or Al Kα radiations, whose energies are 1253.6 eV or 1486.6 eV, respectively. Irradiation produces multiple ionizations from core

and valence energy levels of the irradiated atoms or molecules. XPS is aimed at studying photoemission from core level photoelectrons. The simplified equation describing the photoionization process is [16–22]

$$KE = h\nu - BE \quad (1)$$

in which KE (eV) is the kinetic energy of the photoemitted electron, BE (eV) its binding energy, hν is the X-ray energy (eV). If a positive charge is left on the sample surface by the photoemission process, photoelectrons appear at somewhat lower KE values. The correction of the KE scale is frequently made by referencing to the BE of the 1s energy level of carbon atoms of hydrocarbons present in the sample contamination layer (285.0 ± 0.2 eV). This contamination is usually ascribed to oils from the vacuum system of the spectrometer.

Using UHV conditions is crucial, since (i) it ensures that almost no adsorbed gaseous contaminants cover the solid surface since they could contribute to the XPS signal and (ii) under these conditions, the inelastic mean free path of the electrons (the average distance travelled by electrons through a medium before they are inelastically scattered) is sufficient to allow them leaving the sample and entering in the spectrometer analyzer with unaltered KE). Only photoelectrons leaving the sample without inelastic collision with other atoms or molecules (gaseous molecules adsorbed on the sample surface included) retain their original KE value and give recognizable peak signals. The others, having suffered inelastic collisions, only contribute to the background. In the KE range usually explored (from 500 to 1500 eV) the sampling depth, the depth from which electrons can leave the sample surface without inelastic collisions, ranges between 3 and 10 nm. This means few monolayers, and explains why XPS is an ultimate surface analytical technique. The kinetic energy of the photoemitted electrons is measured by the analyzer and, on knowing hν, it is possible measuring the relevant binding energy, specific of a given core level of the photoemitting atom.

XPS investigations begin with measuring the intensity of photoemitted electrons at any available KE value. The resulting "wide" or "survey" X-ray photoelectron (XP) spectrum displays a series of signals relevant to all electrons photoemitted by energy levels having a BE lower than hν, overlapped to a structured background.

The survey scan in Figure 1, relevant to a glassy carbon electrode (GCE) surface-modified by 8-hydroxyquinoline-5-sulphonic acid (HQSA), evidences (from the right to the left) the signals relevant to electrons photoemitted by the Si 2p, Si 2s, S 2p, Cl 2p, C 1s, N 1s and O 1s energy levels [23].

Survey scans give qualitative information about atoms/molecules present in the sampling depth.

The spectral features at about 950–1050 eV in Figure 1 originate from the decay of core holes left by the photoelectrons. After photoemission from, atoms are left in an unstable excited state (z^{*+}). De-excitation can occur by X-ray fluorescence or by Auger electrons emission. In this last case (see Figure 2), an electron of an outer shell (of energy level L_1) fills the initial core hole (in the energy level K), and this transition makes available sufficient energy for a second electron of an outer shell (of energy level $L_{2,3}$), the Auger one, to be emitted.

The Auger emission is the result of a three-electron process, and leaves the atom doubly-ionized (z^{2+}). Auger decays can continue until inner holes are available.

The Auger region (such as that around 1000 eV in Figure 1) gives access to useful information about the sample composition. It was shown that the energy separation between the two major excursions in the first derivative of the carbon KVV (this notation indicates the second and third electron of the Auger

process are valence band electrons) region can discriminate between sp^2 and sp^3 carbons [24]. Moreover, it is also possible calculating the so-called modified Auger parameter, α', which can also give speciation information and is independent on charging effects [16–22].

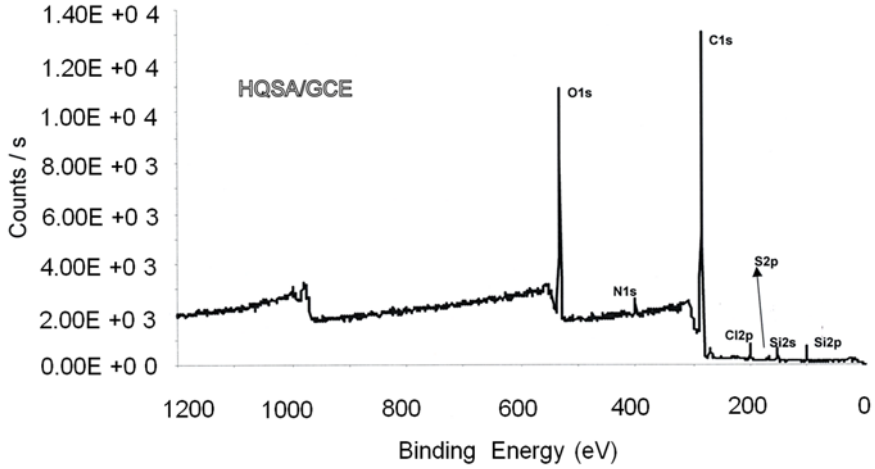

Figure 1. Survey scan relevant to a glassy carbon electrode surface-modified by 8-hydroxyquinoline-5-sulphonic acid (unpublished results from reference [23]).

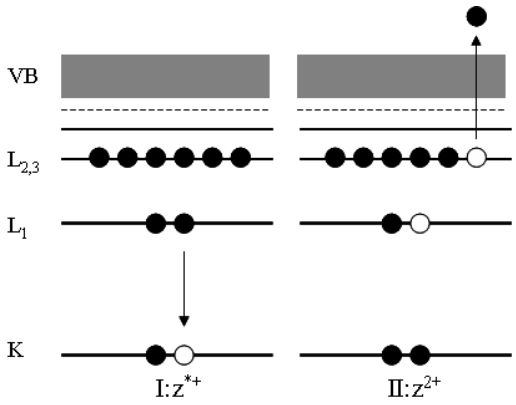

Figure 2. Auger emission steps. I: after core electron emission, the core hole left by photoelectron (o) is filled by an outer electron. II: the energy available from the filling of the initial core hole is used for emitting a second electron, the Auger electron. In this case the Auger electron is named $KL_1L_{2,3}$, or simply KLL. The result is a doubly ionized atom. VB: Valence Band.

The relative intensities of the different photoelectron peaks reflect both the surface atomic abundance and the probability of photoemission from a given energy level. After having identified the elemental composition of the explored surface, it is then possible acquiring "detail" or "high resolution" spectra of any single energy level. An example of detail spectrum relevant to the C 1s region, selected from a previous investigation of ours [24], is shown in Figure 3.

In Figure 3, the experimental (dotted) spectrum is compared with the synthesized (continuous) one, obtained by summing all identified C 1s peak components to the background. Each peak component is assigned to a different type of carbon atom, as shown in Table 1.

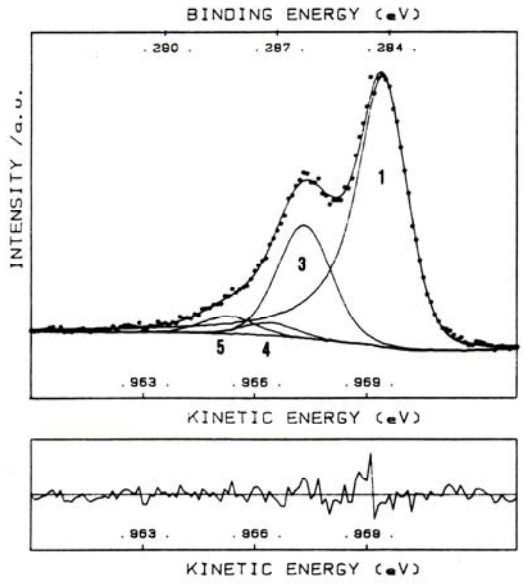

Figure 3. Curve fitting of a C 1s detail scan relevant to a sample of oxidized carbon fibers [24]. Experimental spectrum: dotted curve; synthesized resultant (background + peaks): continuous line. The residual window at the bottom of the figure shows the (properly expanded) difference between experimental and synthesized spectra. The asymmetric peak 1 is assigned to graphitic carbon atoms. Symmetrical peaks 3, 4 and 5 are assigned to C–OH, C=O and O–C=O groups.

Table 1. C 1s binding energies (eV) of some types of carbon atoms [24].

Peak	Carbon Type	BE
1	Graphite, aromatics	284.6
2	Aliphatics	285.1
3	Alcohols, phenols	286.6
3/4	Cheto-enolic groups	287.1
4	Cheto groups	287.9
5	Carboxylic groups	289.3
6	Carbonate, CO_2	290.6
7	Plasmon loss	291.3

Table 1 shows different BE values for the same energy level. This because atoms having a higher positive oxidation state exhibit a higher binding energy due to the extra coulombic interaction between the photoemitted electron and the ion core. Chemical shifts accounts for the difference in BE values of electrons in one specific chemical state of the atom *versus* the value relevant to pure element, or a convenient chemical state of that element. Several papers or handbooks report comprehensive compilations of binding energies values/chemical shifts (see for example references [25,26]).

Photoelectron signals correspond, on a one-to-one basis, to different atomic energy levels. In the simplest case (photoemission from energy levels having quantum number $l = 0$) the signal consists in one peak, more often (if $l > 0$) in a doublet. This is known as spin-orbit splitting (SoS). The theoretical peaks area ratio (PAR) is based on the degeneracy of each spin state of the doublet. In the case of energy levels having quantum number $l = 1$, as in the case of the $2p_{3/2}/2p_{1/2}$ doublet, the PAR is 2/1, while in

the case of the $3d_{5/2}/3d_{3/2}$ doublet the PAR is 3/2 and, in the case of the $4f_{5/2}/4f_{7/2}$ doublet, the PAR is 4/3. SoSs are also important in identifying the correct chemical status of the photoemitting atom.

Each spectral feature can be the envelope of multiple contributions originated by some chemical shifts, as shown in Figure 3. An example of multiple Cr 2p doublets is given in Figure 4 [27].

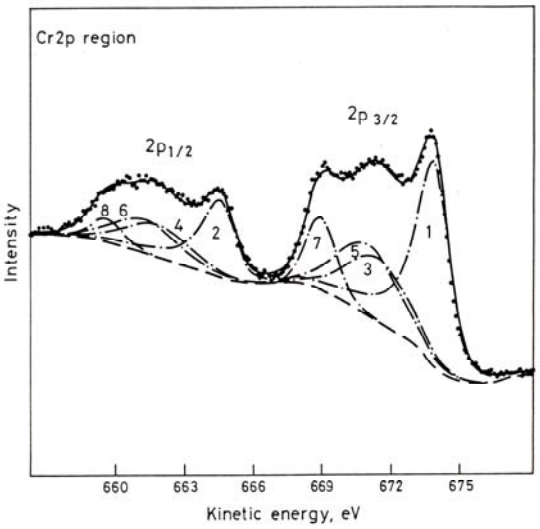

Figure 4. Mg Kα-excited spectrum of the Cr 2p region of a specimen prepared by evaporating potassium dichromate onto a metallic chromium sheet. Doublet 1 + 2: Cr metal; doublet 3 + 4: Cr(III) oxide; doublet 5 + 6: Cr(III) hydroxide; doublet 7 + 8: potassium dichromate [27].

In this figure, the KE scale of the abscissa allows evidencing how the increasing formal positive charge of chromium atoms (from the right to the left of the figure) produces decreasing KEs of photoelectron peaks. Peak positions, full width al half Maximum (FWHM) and SoS data used in curve fitting, reported in eV units, must be chosen in agreement with tabulated values.

Other spectral features are possible, such as shake-up peaks, plasmon loss peaks and satellite peaks, but they are of minor importance in the present context, and are explained in the specific literature [16–22].

Modern XP spectrometers are equipped with dedicated software facilities allowing almost automatic acquisition/processing of XP spectra, and avoiding tedious manual routines. However, often a real good interpretation of the acquired detail spectra requires some interactive adjustment/interpretation.

So, while survey scans allow performing a qualitative analysis, detail scans allow a sort of speciation analysis, being capable of discriminating between atoms characterized by a different charge/chemical surrounding. Moreover, a proper measurement of peak areas allows performing at least a semi-quantitative analysis. On considering that this information is relevant to few surface monolayers, XPS is invaluable in corrosion, adhesion and catalysis investigations.

From what above reported, XPS represent a favorable choice in CMEs investigations, since the very surface of an electrode determines its electrochemical performances. However, some caution is necessary, since the chemical status of the CME surface can undergo more or less heavy degradations, when transferred to UHV working conditions and/or under X-ray irradiation. Moreover, it is necessary considering that instruments are very expensive, so that accessibility cannot be very easy.

These problems justify some hesitation towards exploiting XPS in CMEs investigations. Nonetheless, according to our previous experience (see for example references [23,28–30]) XPS can give precious or otherwise unavailable information in CMEs investigations.

3. Survey of Literature Information

The papers examined in this review can hardly be grouped according to some rigid criteria since, often, their topics and experimental approaches are often more or less overlapped. For this reason, they are here grouped in three sections according with the explored spectroscopic regions. The first section includes papers in which XPS characterization was mainly focused at exploring C 1s and/or O 1s and/or N 1s regions [31–52]. The second includes papers in which the spectroscopic regions of a specific element were explored [53–70]. In the last one, a more comprehensive analysis of the spectroscopic regions of multiple elements is involved [71–112]. In all cases, the BEs of some of the explored regions are reported to allow a better understanding of XPS performances.

3.1. C 1s, N 1s and O 1s Regions

Lakard *et al.* performed a SEM/XPS/PM-IRRAS study aimed at developing functionalized polypirrole (PPY) films suitable as sensitive layers for pH sensors [31]. The sensors were obtained by potentiostatic electrodeposition of poly(11-N-pyrrolylundecanoic) acid (PPUA) or poly(N-undecylpyrrole) (PUP) on Pt working electrodes. XPS survey spectra of the two CMEs evidenced the presence of carbon, nitrogen, oxygen and chlorine. The absence of signals attributable to platinum confirmed the presence of compact surface polymer layers. C 1s survey scan of PPUA/Pt modified electrodes evidenced the presence of five contributions. They were assigned to carbon atoms of the heteroaromatic ring (284.2 eV), aliphatic carbons from the ten-carbon alkyl chain grafted on the nitrogen of pyrrole monomers (284.8 eV), carbon atoms of C–N^+ (285.8 eV) and C=N^+ (287.3 eV) groups and carbon atoms of –COOH grafted on the alkyl chain (289.5 eV). Similar peak contributions, with the exception of that assigned to carboxylic carbons, were evidenced in the case of the PUP/Pt electrode. The characterization of the surface of the two sensors was completed by the analysis of the N 1s and Cl 2p regions. The CMEs were tested as potentiometric pH sensors in aqueous media. The best potentiometric response, observed at PPUA based sensors, were ascribed to the reversibly protonable carboxylic acid groups.

Hu *et al.* prepared a carboxyl ion implantation-modified indium tin oxide (ITO) electrode suitable for the determination of pirarubicin [32]. $COOH^+$ ions to be implanted onto the ITO surface were obtained by ionizing gaseous formic acid accelerated in an 80 keV electric field. The COOH/ITO electrode was characterized by XPS. After the $COOH^+$ ion implantation, the C 1s detail scan was fitted by four peaks. They were assigned to carbon atoms of C–C/C–H bonds (284.80 eV), of C–OH groups (286.30 eV), of C=O groups (287.00 eV) and carboxyl groups (289.38 eV), thus demonstrating that $COOH^+$ ions were successfully implanted onto the ITO surface and that they maintained the characteristics of the carboxyl group. The electrochemical performances were explored by CV and Differential Pulsed Voltammetry (DPV). Compared to the bare ITO electrode, the CME exhibited a marked enhancement in the current response to pirarubicin. The COOH/ITO electrode was applied to its determination in water samples.

Zhao *et al.* synthesized water-soluble poly(diallyldimethylammonium chloride)–graphene nanosheets (PDDA–GR_{NS}) [33]. PDDA–GR_{NS} were characterized by UV–Vis absorption spectroscopy, XRD and XPS. XP spectra of graphite oxide (GO), from which graphene was obtained by chemical reduction, were compared to those of PDDA–GR_{NS}. The C 1s region of GO was fitted by three peaks, assigned to C–C (284.8 eV), C–O (286.8 eV) and C=O (288.6 eV) groups. After the reduction to GR_{NS}, the peak corresponding to C–C became predominant, while the others markedly decreased, indicating the removal of oxygen-containing functional groups. PDDA-GR_{NS} were used for constructing different types of gold nanoparticles/graphene nanosheets hybrid nanocomposites by one-pot synthesis, *in situ* reduction and adsorption methods. GR_{NS}-based nanocomposites dispersions were dropped onto the surface of GCEs. The electrocatalytic activity of the Au_{NP}/PDDA–GR_{NS}/GCE was evaluated in neutral phosphate buffer solution (PBS) containing uric acid (UA). CV results showed that the anodic peak current of UA at the CME was two-order of magnitude higher than that obtained at bare GCEs. DPV was used to determine UA quantitatively in buffer solution and urine samples, even in the presence of adrenaline.

Sundaram and Annamalai studied the electroxidation of phenol and its derivatives (o-cresol and p-cresol) at several carbon nanotubes (CNT)-modified GCE in neutral PBS [34]. Hydroquinone (HQ), a by-product of phenol oxidation, was selectively immobilized on the surface of a GCE modified with purified multiwalled carbon nanotubes (p-MWCNT/GCE) as well as on screen-printed gold electrodes (SPEAu). The TEM, FTIR and XPS characterization of the HQ/p-MWCNT hybrid material evidenced the presence of unreacted phenol on its outer surface, and of clusters of HQ and of HQ-biphenol species inside its walls. This was in agreement with the fitting of C 1s and O 1s regions, which evidenced the existence of significant amount of oxygen functionalities on the p-MWCNT surface. This finding suggested the formation of carbon rich organic compounds, phenol and HQ at the interface of the p-MWCNT. CV and in-situ EQCM measurements at HQ/p-MWCNT/GCEs allowed evidencing a highly selective electrocatalytic oxidation of hydrazine through the mediation of the immobilized HQ/quinone redox species, without any interference from cysteine, ascorbic acid, uric acid, dopamine, nitrite, nitrate and hydrogen peroxide. Most interestingly, the CME exhibited a twice-higher antibacterial activity towards *Escherichia coli* bacteria over the native phenol, thus suggesting potential applications as hydrazine sensor and thin-film based antibacterial agent.

Fu *et al.* performed a CV/SWV/DPV/SEM/TEM/XRD/FTIR/XPS investigation aimed at developing electrocatalytic sensors based on C60 microspheres [35]. SEM pictures showed that microspheres were hollow structures. TEM images showed that microspheres turned to solid microrods after ethanol addition. Raman, XRD and FTIR spectra allowed determining the composition and crystalline nature of hollow spheres and solid rods. XP spectra of the C 1s region of C60-film modified electrodes were fitted by components assigned to non-oxidized carbon (284.7 eV), to C–OH (286.5 eV) and to C−O− (289.0 eV). C60 microsphere-modified gold and glassy carbon electrodes (C60/Au and respectively C60/GCE) were tested as DPV and SWV sensors for dopamine, ascorbic acid, L-cysteine, and uric acid. Because of their porosity and hydroxylation, C60 films displayed a high affinity for the tested biomolecules, so that C60 modified electrodes could be proposed as sensitive sensors for the highly selective testing of the four analytes. These performances suggested the possibility of broad applications in the fullerene nanotechnology.

M. Carbone *et al.* performed a CV/CA/SEM/TEM/FTIR/XPS study aimed at modifying screen-printed electrodes (SPEs) by graphene oxide (GO) nanoribbons/ionic liquid (IL) dispersions [36]. Explored ILs were 1-butyl-3-methylimidazolium chloride (BMIM-Cl) or 1-butylpyridinium chloride (Bupy-Cl). XPS was used to characterize GO powder before and after dispersion in BMIM-Cl and Bupy-Cl. The C 1s and O 1s regions of these specimens were practically the same. The C 1s region of GO dispersed in BMIM-Cl was fitted by three peaks assigned to aromatic carbon (284.7 eV), to C–O (286.3 eV) and to carbon bonded twice to hydroxylic groups (288.1 eV). Nitrogen was absent. FTIR findings confirmed the absence of carbonyl and/or carboxyl groups. The electrochemical detection of several molecules ($Fe(CN)_6^{3-}$, Na_3IrCl_6, $Ru(NH_3)_6^{3+}$, ascorbic and caffeic acid, dopamine, NADH and others) was tested by comparing the CV results obtained at GO/IL-modified SPEs, GC and HOPG electrodes. Based on the overall results, it was concluded that GO/ILs/SPE electrodes, characterized by the best electrochemical performances, could be applied for assembling various biosensors.

Zhai *et al.* synthesized polyaniline (PANI) and copolymers of aniline with m-nitroaniline (poly(aniline-co-m-nitroaniline)), in various molar ratios of co-monomers, by chemical and electrochemical polymerization [37]. The UV-Vis spectra of PANI and of copolymers powders, measured in DMF, allowed verifying the meta-coupling of m-nitroaniline with aniline. It was shown that m-nitroaniline could polymerize by potential cycling on a PANI/GC electrode to generate the polyaniline/poly(m-nitroaniline) composite. XPS survey scans relevant to polyaniline/ poly(m-nitroaniline)/GCE evidenced only the C 1s, N 1s and O 1s regions. The N 1s region was fitted by four components assigned to nitrogen atoms of nitride –N= (398 eV), amine –NH– (400.0 eV), doped imine $–NH^+–$ (402.00 eV) and nitro groups $–NO_2$, (405.22 eV). Oxygen and carbon percents obtained by XPS, allowed obtaining the proportion of m-nitroaniline in the polymers (22.7%) corresponding to 2.27 molecules m-nitroaniline polymerized on 7.73 molecules polyaniline after 50 cycles. The possibility of polymerizing m-nitroaniline on PANI could be used to remove m-nitroaniline from aqueous solutions.

Toppare *et al.* modified graphite electrodes with poly(2-(2,5-di(thiophene-2-yl)-^{1}H-pyrrol-1-yl) (SNS-acetic acid) [38]. The CME was subsequently functionalized with lysine (Lys) and with two poly(amidoamine) (PAMAM) derivatives (PAMAM G2 and PAMAM G4). The XPS characterization of the modified layers allowed determining the amide bond formation between carboxylic acid groups of the polymer and amine groups of Lys, PAMAM G2 and PAMAM G4. The C 1s region of the Lys immobilized surface was fitted by five peaks, one of which (287.84 eV) was assigned to amide bond (–N–(C=O)) between polymer and Lys molecules. The relevant N 1s region was fitted by two peaks assigned to $–NH_2$ (398.43 eV) and –N–(C=O) (400.50 eV). Similar analyses were reported about the other modified electrodes and the biomolecules immobilized their surfaces. The surface morphology of the CMEs was explored by AFM. The amino groups of Lys, PAMAM G2 and PAMAM G4 favored the subsequent immobilization of glucose oxidase (GOD) using glutaraldehyde (GA) as the crosslinker. The GOD-modified CMEs were characterized by CV and amperometric studies in acetate buffers containing variable glucose concentrations and in human blood serum samples.

Hong *et al.* described a Prussian blue (PB)-modified electrochemical sensor based on chitosan (CS)-functionalized graphene nanosheets [39]. Graphene (rGO) was obtained by reduction of graphite oxide (GO). The morphology and composition of the rGO-CS/PB nanocomposite sheets were characterized by TEM, XPS and XRD. TEM images showed the high-loading and uniform distribution

of the PB nanocubes on the nanocomposite. XPS was used for comparing the C 1s regions of GO and rGO-CS/PB samples. The C 1s region of GO was fitted by four components assigned to C–C (284.6 eV), C–O (286.7 eV), C=O (287.6 eV) and O–C=O (288.7 eV) carbons. After the chemical reduction to rGO, all three peaks assigned to oxygenated functionalities significantly diminished, suggesting the occurred deoxygenation, and a new C 1s peak was assigned to C–N bonds (285.7 eV), thus confirming the combination of chitosan with graphene nanosheets. Hydrogen peroxide sensors were the prepared by drop-casting, in sequence, rGO-CS/PB and Nafion© (NA) solutions on the surface of GCEs. The electrochemical behavior of the resulting NA/rGO-CS/PB/GCE was investigated by CV and amperometry. The CME showed a good electrocatalytic activity for the reduction of H_2O_2. The amperometric detection was unaffected by the presence of ascorbic acid, cysteine, and citric acid.

Zen *et al.* described the electrochemical synthesis of electroactive poly(melamine) (PMEL) and its application to prepare nanotubes–nanoparticles hybrid [40]. CV measurements allowed defining the best polymerization parameters. The as synthesized PMEL was characterized by XPS. The N 1s region was fitted by four peaks assigned to imine nitrogen at the ring (398.5 eV), neutral amine nitrogen (399.5 eV), delocalized polaron-type nitrogen (400.8 eV) and positively charged protonated amine nitrogen (402.2 eV) atoms. Screen-printed carbon electrodes (SPCE) were activated (SPCE*) by pre-anodization in PBS. MWCNT were also activated in an acidic medium. The activated MWCNT were drop coated on SPCE* (MWCNT-SPCE*). Melamine was then polymerized on the MWCNT-SPCE* by potential cycling. At last, copper was electrodeposited on the PMEL-functionalized MWCNT-SPCE*. SEM images showed that copper nanoparticles were present as flower-like clusters on the surface of the PMEL-modified MWCNT. The described functionalization with PMEL was proposed as a methodology for preparing new materials to be applied in different fields.

Jeon *et al.* described an electrochemical sensor for H_2O_2 based on electrochemically reduced graphene oxide (ERGO) grafted with aminothiophenol (ATP) and covalently bonded to palladium nanoparticles [41]. The ERGO-ATP-Pd_{NP} composite was characterized by TEM, XPS, EDS and EIS. Survey and detail XPS scans were acquired of the ERGO–ATP–Pd_{NP} composite and of its GO, GO-ATP, GO-ATP-Pd_{NP} precursors. The S 2p (168.92 eV) and N 1s (400.1 eV) signals in the survey spectra proved the attachment of the ATP to ERGO. The Pd $3d_{5/2}/3d_{3/2}$ doublet (336.3/341.6 eV) in the same spectra confirmed the attachment of Pd_{NP}. The C 1s signals of the four samples were fitted by the same three peaks (in different intensity ratios) assigned to C–C and C=C (285.0 eV), to C–O and to C=O carbon atoms. O 1s spectra of the fabricated ERGO-ATP-Pd_{NP} evidenced a heavy deoxygenation, indicating the efficient ATP combination with GO. The H_2O_2 sensor was obtained by coating GCEs with the composite. CV and chronoamperometry (CA) results showed that ERGO-ATP-Pd_{NP}/GCEs were characterized by a favorable catalytic activity. The sensor could be applied to the direct detection of hydrogen peroxide and indirect detection of hydrogen peroxide generated from enzyme reactions, for example for the determination of glucose.

Raj and John reported the fabrication of ERGO films on glassy carbon electrode by a self-assembly method [42]. GCEs were immersed into a solution of 1,6-hexanediamine (HDA). GO was self-assembled on HDA/GCEs via electrostatic interaction between positively charged amine groups and negatively charged carboxyl groups of GO. GO/HDA/GCEs were electrochemically reduced in neutral PBS obtaining the final ERGO/HDA/GCE. The reduction was confirmed by ATR-FTIR and Raman spectroscopies, XRD, XPS, AFM and SEM by using ITO as a substrate. C 1s XP spectra of

GO/HDA/ITO were fitted by six peaks assigned to sp^2 carbons (284.5 eV) and to C–N (285.3 eV), C–OH (285.4 eV), C–O (286.4 eV), C=O (287.6 eV) and O–C=O carbons (288.4 eV). After the reduction to ERGO/HDA/ITO, the peaks assigned to C=O and O–C=O carbons were absent. The increase of the C/O atomic ratio from 1.18 to 4.32 confirmed the removal of oxygen functionalities from the GO surface. CV and DPV measurements confirmed the electrocatalytic activity of the ERGO/HDA/GCE towards ascorbic acid, dopamine, and uric acid.

Guo *et al.* described the modification of carbon surfaces with neutral red (Nred) from its diazonium salts [43]. The immobilization of Nred onto GCEs was achieved by immersion in a Nred–$NaNO_2$–HCl solution via the spontaneous reduction of in-situ generated Nred diazonium salts. The Nred/GCEs were characterized by CV, AFM and XPS. XPS allowed evidencing significant differences between the surface of electrodes simply modified by Nred physical adsorption and that of spontaneously modified electrodes. The N 1s peak of physically coated surfaces was fitted by two peaks assigned to imine –N= and amine nitrogens (399.1 eV) and to positively charged nitrogen atom in $=N^+(CH_3)_2$ groups (400.0 eV). The N 1s region of the spontaneously modified surfaces, besides the previously mentioned peaks, exhibited a third one assigned to nitrogen in NO_2^- groups (401.5 eV), likely electrostatically attracted by the positive $=N^+(CH_3)_2$ groups in the Nred molecule. The effects of Nred modification via spontaneous reduction was tested by monitoring the current generated during microbial anodic acetate oxidation. In this test, high specific surface area graphite felts replaced GCEs for allowing faster responses. The results demonstrated the effectiveness of the covalently bound Nred as insoluble redox mediator during the microbial anodic oxidation of acetate ions.

Ghilane *et al.* investigated the immobilization of dopamine (DA) onto macroelectrode and microelectrode surfaces by one–step oxidative grafting and, alternatively, by a stepwise grafting combining diazonium grafting and peptide coupling [44]. The electrochemical characterization of GC and carbon fiber DA-modified electrodes, performed by CV in acidic media, evidenced the presence of the o-dopaminoquinone/DA redox signal, and that the attached DA layer was a few nanometers thick. FTIR and XPS experiments were performed by using gold in place of carbon substrates. FTIR results of the DA-modified gold substrate indicated the presence of carbonyl groups whatever the grafting method, and confirmed the conversion of the attached DA layer to o-dopaminoquinone upon anodic polarization. XPS survey scans acquired after the grafting procedures were consistent with the covering of the gold surface. The C 1s detail spectra of the DA-modified gold substrate was fitted by three peak assigned to C–H or aryl species (284.6 eV) and to C–O (286.5 eV) and C=O (288.6 eV) carbons. The N 1s peak (400 eV) was assigned to N−H groups. The DA-modified electrodes exhibited a fast electron transfer, with lower ΔE_p than the majority of pretreatment procedures. Moreover, the ΔE_p was as small as that observed for more complex surface treatments.

Raj and John described the determination of allopurinol (AP) using a GCE modified by ERGO nanosheets and 1,6-hexanediamine (HDA) [45]. Preparation and characterization of the CME were described in a previous paper [42]. As in that paper, XPS measurements were performed by using ITO as a substrate in place of GC. XP spectra relevant to the O 1s region of GO/HDA/ITO and ERGO/HDA/ITO evidenced the significant reduction of oxygen surface functionalities after the electrochemical reduction. Evaluating the effect of AP in body fluids after gout treatments required the simultaneous determination of AP and UA. The electrochemical performances of the GCE based sensor towards the oxidation of allopurinol, ascorbic acid (AA) and uric acid (UA) were investigated by CV,

amperometry and DPV in pH 7.2 PBS. Enhanced oxidation currents of the three analytes were observed at the ERGO/HDA/GCE in comparison to those relevant to GCE and GO/GCE. The ERGO film effectively prevented surface fouling effects. The described sensor was applied to the simultaneous measurement of AP, UA and AA in human blood serum, urine samples and commercial tablets.

Toppare *et al.* synthesized the new monomer 2-(4-nitrophenyl)-4,7-di(thiophene-2-yl)-^{1}H-benzo[*d*]imidazole (BIPN) [46]. The BIPN was then sonicated with functionalized MWCNT (f-MWCNT). The final CME was obtained by potential cycling of a GC rod in the BIPN/f-MWCNT suspension. The final enzyme electrode was then obtained by spreading onto the modified electrode a solution of alcohol oxidase (Aox), N-(3-dimethylaminopropyl)-N-ethylcarbodiimide hydrochloride (EDC) and N-hydroxysuccinimide (NHS). The modified electrode was characterized by SEM, XPS and FTIR techniques. XPS was used to monitor the evolution of surface functionalities in pristine MWCNT, f-MWCNT, poly-BIPN (PBIPN), f-MWCNT/PBIPN and Aox/f-MWCNT/PBIPN. The C 1s region of the MWCNT and f-MWCNT was fitted by peaks assigned to C–C and C=C (284.8 eV), C–O and C=O (286.4) and, after the functionalization, to O=C–O (288.7 eV). After the immobilization of Aox, the C 1s region was characterized by an intense peak assigned to C–N bond, imidazole, nitrobenzene (285.2 eV) and by the increase of a peak at 288.2 eV, assigned to carboxylic groups of f-MWCNT and protein molecules. At last, the peak at 287.1 eV could be assigned to O=C–N bonds, thus confirming the covalent immobilization via amide bond. The increase of the signal at 288.2 eV confirmed the presence of carboxylic acids due to f-MWCNT and protein molecules. The electrochemical responses of the enzyme electrode were amperometrically evaluated by monitoring oxygen consumption in the presence of ethanol. The biosensor was successfully applied to the determination of ethanol in some beverages.

Hao *et al.* described the synthesis of poly(3,4-ethylenedioxythiophene)/graphene oxide (PEDOT/GO) composites by *in situ* potentiostatic polymerization of monomer and GO, without additional dopants [47]. The morphology and structure of PEDOT/GO film was characterized by TEM, Raman and XPS. TEM images of the PEDOT/GO film showed GO sheets uniformly covered by PEDOT nanodots. A fit of the C 1s photoelectron region allowed an approximate identification of surface functionalities of the composite. The electrochemical performances of a CME, prepared by potentiostatically depositing PEDOT/GO onto a GCE, were explored by CV and DPV. Compared with the GO modified electrode, the cyclic voltammograms at the PEDOT/GO/GCE showed a better reversibility and a lower ΔE_p, proving that PEDOT improved the electrocatalysis of the composite toward the redox behavior of acetaminophen. DPV measurements showed that the sensor could determine acetaminophen without interferences from AA and DA. The sensor was applied to the analysis of acetaminophen in Paracetamol tablets and urine samples.

You *et al.* proposed a method for preparing ERGO [48]. The morphology and structure of ERGO were characterized by SEM, XPS, Raman and XRD. SEM images showed that the relatively smooth surface of GO became rougher and wrinkled after reduction. The fitting of the C 1s XPS region of GO and ERGO allowed evidencing a consistent decrease of the intensity of C 1s peaks assigned to carbon atoms bound to oxygen after the electroreduction. ERGO/GCEs were obtained by potential cycling of GO/GCEs in neutral PBS. The electrochemical performance of ERGO/GCE were compared to those of a bare GCE in solutions containing $Ru(NH_3)_6^{3+/2+}$, $Fe(CN)_6^{3-/4-}$ and $Fe^{3+/2+}$ probe molecules. The superior performance of ERGO/GCE were ascribed to larger electroactive surface area, more numerous edge plane defects and residual oxygen-containing groups. CV and DPV measurements

allowed showing a higher electrocatalytic activity of ERGO/GCE toward the oxidation of DA, AA and UA. The CME was applied to the analysis of DA in urine samples.

Liu, Gooding *et al.* investigated the influence of graphene nanosheets (GR_{NS}) on the electrical communication through organic layers fabricated on graphite and gold electrodes [49]. The stepwise modification of the two electrode substrates (ES) was performed with benzoic acid (BA/ES), followed by pyrene (Py-BA/ES) and then GR_{NS} via π-π stacking interaction (Gr_{NS}-Py-BA/ES). The CMEs were characterized by SEM, AFM, EIS and XPS. XP spectra were acquired throughout the step-wise modification procedure by monitoring the C 1s, O 1s and N 1s regions. The weak N1s peak (400 eV) of the Gr_{NS}-Py-BA/GE was assigned to amide bonds. The C 1s region of the same CME was dominated by the graphitic carbon (C–C/C=C) peak (284.4 eV). Other C 1s peaks were assigned to C–N (285.0 eV) and –CO–NH– (288.2 eV) groups, thus supporting the successful attachment of Py, and to carboxylic O=C–O (288.8 eV) and ether C–O–C (286.1 eV) groups. The electrochemistry of the CMEs at different stages of modification was studied in the presence of the $Fe(CN)_6^{3-/4-}$ redox probe. CV experiments proved that the attachment of graphene nanosheets lowered the interfacial electrochemical impedance by forming conducting pathways through the passivating monolayer, and that Faradaic electrochemistry could occur between the redox probes and the underlying electrode.

Wei, Chen *et al.* developed a sensor based on a GCE surface modified by a film of overoxidized polyimidazole (PImox)/graphene oxide copolymer [50]. The copolymer was characterized by SEM, AFM, FTIR, XPS and EIS. TEM and SEM images evidenced that the GO nanosheets were covered with a porous PImox film. The surface chemistry of the sensor was characterized by comparing XPS spectra of polyimidazole-GO and PImox-GO composites. The C 1s region of the two films was fitted by four peaks assigned to sp^2 carbons (285.0 eV) and C–O (286.4 eV), C=O (287.84 eV) and O–C=O (289.14 eV) bonds. The comparison showed a clear increase of oxygenated functionalities after the overoxidation. CV and DPV experiments allowed testing the electrochemical performances of the sensor, which exhibited a remarkable electrocatalytic activity toward the oxidation of ascorbic acid, dopamine, uric acid, guanine and adenine in acidic PBS buffers. The effect of pH on the results of the DPV analysis of the four analytes was explained as a function of the relevant pK_a values. The promising overall performances of the sensor were ascribed to the synergic coupling of GO and PImox, which allowed resolving their oxidation peaks into five well-defined peaks.

Raghupathy, Jeong, Grace *et al.* developed a Cu_2O nanocubes-modified glassy carbon electrode (Cu_2O_{NC}/GCE) by drop casting a cuprous oxide/Nafion® homogeneous solution onto the GCE surface [51]. Cu_2O_{NC} were characterized by XRD, FESEM, XPS and DRS-UV. SEM and XRD results evidenced the cubic structure of the synthesized Cu_2O nanoparticles. The XPS survey scan evidenced the C 1s, O 1s and Cu 2p regions. The Cu $2p_{3/2}$/$2p_{1/2}$doublet (932.5 eV/952.4 eV) was consistent with Cu_2O, as also evidenced by XRD data. The O 1s peak was fitted by three components assigned to Cu_2O (530.1 eV), hydroxyl groups (531.4 eV) and adsorbed molecular water (533 eV). The electrochemical performances of the CME, evaluated by CV, chronoamperometry and EIS in NaOH solutions, showed that the Cu_2O_{NC}/GCE exhibited a high electrocatalytic activity towards glucose oxidation compared with bare GCE electrode, without interferences from molecules like UA, AA and DA. The sensor was applied to the determination of glucose in human urine by standard addition method.

3.2. Metal/Nonmetal/Metalloid Regions

Jousselme *et al.* performed a CV/LSV/SEM/^{1}H-NMR/FTIR/XPS investigation aimed at functionalizing multi-walled carbon nanotubes electrodes with ferrocene derivatives [52]. The immobilization of the ferrocene moiety via π-π interactions was made by mean of a new ferrocene derivative bearing a pyrene group. Alternatively, the covalent grafting on the film of CNTs was obtained via the electroreduction of an aminoethylbenzenediazonium salt followed by post-functionalization with an activated ester derivative of ferrocene. Attachment of ferrocene was proved by the presence of a CV reversible oxidation wave. The large peak-to-peak separation and high capacitive current were explained by the significant resistivity and the 3D morphology of the CNT network. The CME was characterized by XPS. The Fe 2p region in XPS survey scans of electrodes modified by ferrocene bearing a pyrene group confirmed the presence of ferrocene at the MWCNT surface and, in particular, the presence of Fe(II). As a first application, the sensor was applied to glucose biosensing in the presence of glucose oxidase.

Taghavinia *et al.* performed a SEM/LSV/DRS/XRD/XPS investigation aimed at preparing nanostructured silver electrocatalysts suitable for oxygen reduction in basic media [53]. Silver was deposited on the surface of cellulose fibers. Subsequently, the cellulose template was heat removed to obtain self-standing nanostructured silver fibers (NSSFs). The NSSFs were then incorporated in a graphite composite electrode. The chemical composition of the fibers was monitored before and after heat treatment by using XPS analysis. In particular, the Ag $3d_{5/2}$ region relevant to heat-treated fibers was resolved into two components (368.4/367.5 eV) assigned to silvery cellulose fibers and to silver fibers (Ag(0) and AgO, respectively) thus showing that the heat treatment of the silvery cellulose fibers at 400 °C caused the partial oxidation of the Ag fibers surface. The electrocatalytic properties of the sensor were tested by LSV experiments in saturated oxygen solutions. The NSSFs modified GCEs exhibited a higher negative current density and/or more positive onset potential of the oxygen reduction reaction, confirming the better electrocatalytic performance of the proposed CME with respect to bare GCEs.

Yuan *et al.* developed a glucose biosensor based on the immobilization of glucose oxidase (GOD) on a multilayered CME [54]. The sensor was obtained by subsequently depositing onto the surface of the GCE a Prussian blue–multiwalled carbon nanotubes (PB-MWNTs) dispersion, a hollow PtCo (H-PtCo) nanochains solution, a GOD solution and, at last, a Nafion® layer (this last to prevent possible enzyme leakage and eliminate foreign interferences). The composite was characterized by UV-Vis/FTIR/SEM and XPS parallel techniques. XPS, in particular, allowed verifying the presence of the Pt-Co alloy in the multilayered surface film. The higher BE of the Pt $4f_{7/2}$ peak (71.5 eV), relevant to the NA/GOD/H-PtCo/PB-MWNT/GCE with respect to that of pure Pt(0) (71.2 eV), was attributed to the alloy formation with cobalt. EIS, CV and chronoamperometric measurements allowed testing the good analytical performances of the biosensor towards glucose. Moreover, the biosensor response was not affected by dopamine, glycine, l-cysteine, ascorbic acid and ethanol. The proposed modification performances could be exploited in developing other amperometric enzyme biosensors.

Guascito *et al.* performed a CV/UV-Vis/PAD/XPS investigation aimed at preparing a non-enzymatic electrochemical sensor for glucose detection [55]. The CME was obtained by drop casting a dispersion of Ag_{NP} capped in PVA on a Pt electrode. The Ag_{NP}/PVA/Pt modified electrode was

characterized by XPS. Survey scans of the Ag_{NP}/PVA/Pt modified electrode evidenced the presence of N 1s and Ag 3d signals. Detail scans of the Ag 3d region were fitted by two doublets. A first Ag $3d_{5/2}$ peak was attributed to Ag(0) in the nanometer size, as its BE (369.0 eV) was significantly higher than that for bulk Ag (368.0 eV). The second, minor component (367.5 eV) was assigned to unreacted $AgNO_3$. CV and PAD measurements, performed for checking the response of the Ag_{NP}/PVA/Pt sensor to glucose, allowed confirming its sensitivity at very low analyte concentrations. The developed electrochemical sensor was proposed as a prototype of advanced *in vivo* glucose sensors and as a valid alternative to classical glucose (bio)sensors.

Guascito *et al.* also performed a CV/CA/SEM/EDX/XRD/XPS investigation aimed at developing an amperometric H_2O_2 sensor by drop casting an ethanol dispersion of Te-microtubes (TeμT) on a Pt electrode [56]. XPS was used to characterize as synthesized TeμT and TeμT/Pt electrodes, either before or after being cycled in PBS. Before the CV treatment, high-resolution spectra of the Te 3d region of TeμT and TeμT/Pt electrodes were fitted by three components. The most intense $3d_{5/2}$ peaks were assigned to Te(0) (573.3 ± 0.1) and Te(IV) (576.6 ± 0.1 eV). The third peak, assigned to Te(VI) (577.8 ± 0.1) disappeared after the electrochemical treatment, confirming that this species was not stable in pH 7.0 PBS. CV experiments in neutral PBS showed that the Te-microtubes of the CME were responsible for an increment of both cathodic and anodic currents in presence of H_2O_2 with respect to those obtained at bare Pt. The results of amperometric experiments in batch and in FIA proved the suitability of the TeμT/Pt electrode for the quantitative determination of H_2O_2.

Li *et al.* modified a glassy carbon electrode by Pd nanoparticles-decorated multiwalled carbon nanotubes (Pd/MWNT) [57]. The morphology and composition of the Pd/MWNT catalyst were characterized by TEM, EDX and XPS. TEM images showed that Pd nanoparticles were loaded on the multiwalled carbon nanotubes microparticles. The survey XPS scan of the Pd/MWNT composite evidenced the C 1s, O 1s and Pd 3d regions. The main Pd $3d_{5/2}$/$3d_{3/2}$ doublet (334.6 eV/339.9 eV) was assigned to Pd(0). Combined with those of TEM and EDX, these results proved that the Pd(0) nanoparticles were successfully deposited on the MWNT. CV measurements showed that the Pd/MWNT/GC modified electrode displayed a high electrocatalytic activity towards the reduction of bromate ions. Chronoamperometric measurement confirmed that the CME could be successfully employed as an amperometric sensor for bromate in a wide concentration range. This confirmed that Pd/MWNT/GCEs have potential applications as bromate detector.

Guascito *et al.* developed a non-enzymatic amperometric sensor for glucose detection based on a Pt electrodes modified with Te microtubes [58]. TeμT powder and TeμT/Pt electrodes were characterized by SEM and XPS. SEM measurements showed that the as-synthesized TeμT were characterized by a tubular structure with hexagonal cross-section and open ends. XPS involved the acquisition of C 1s, O 1s, Pt 4f and Te 3d regions. The Te $3d_{5/2}$ region of TeμT/Pt electrodes cycled in PBS was fitted by three components assigned to Te(0) (573.4 ± 0.1 eV), Te(IV) oxide (BE = 576.7 ± 0.1 eV) and Pt/Te(II) adsorbed species (BE = 575.7 ± 0.1 eV). The Te(0) component was in good agreement with that of pure Te(0) (573.4 ± 0.1 eV). The electrochemical characterization of the TeμT/Pt CME was performed by CV and chronoamperometry in neutral PBS. According to electrochemical results, the proposed sensor exhibited strong and sensitive amperometric responses to glucose. The CME proved suitable as non-enzymatic sensor for glucose detection using low working potentials at physiological pH.

Jeyadevan *et al.* proposed a method for synthesizing CuO nanoleaves (CuO_{NL}) in the presence of the poly(diallyldimethylammonium chloride) (PDDA) cationic polyelectrolyte [59]. Structure and morphology of CuO_{NL} were characterized by FT-IR/XRD/XPS/TEM and FESEM. XRD results relevant to PDDA stabilized CuO_{NL} confirmed the formation of a monoclinic CuO structure. The XPS survey scan evidenced the presence of carbon, oxygen and copper. The Cu $2p_{3/2}/2p_{1/2}$ doublet (933.8 eV/953.8 eV; SoS 20 eV)) was assigned to CuO. The O 1s peak was fitted by three peaks, assigned to CuO (529.4 eV), O–O (530.6 eV) and OH– (532.2 eV). The CuO_{NL} were drop-casted onto a MWCNT/GCE and tested as a sensor of norfloxacin. CV and DPV experiments allowed comparing its oxidation behavior at CuO_{NL}/MWCNT/GC, MWCNT/GC and bare GC. CV measurements showed the irreversibility of norfloxacin electroxidation at the CME and that the electrode process was controlled by the adsorption of the analyte. The presence of CuO_{NL} onto the CME surface allowed an enhanced oxidation of norfloxacin with respect to a copper-free MWCNT/GCE.

Kim *et al.* described an electrochemically active organosilane linkage, with cyclic disulfide (CDSI) as an end functional group, as a modifier of ITO electrode surfaces through a self-assembly process [60]. The subsequent anodic oxidation of CDSI/ITO electrode allowed activating disulfide-functionalities for further surface-immobilization reactions. XPS was used to characterize the CME surface before and after anodic oxidation. Before the oxidation, the S $2p_{3/2}/2p_{1/2}$ doublet (163.5 eV/165.0 eV) was assigned to –S– groups. After the oxidation, an additional peak was observed (167.5 eV), compatible with the presence of oxides of sulfur, thus suggesting the conversion of disulfide into its oxidized thiosulfinate and thiosulfonate species. Fluorescence microscopy allowed showing that the CME could be used for immobilizing thiol-ended molecules with high spatial selectivity and for detecting biomolecules with high specificity, including DNA, peptides, nanomaterials as well as proteins. After electrochemical oxidation, a CDSI-modified microelectrode array was treated with freshly prepared, cleaved anti-rabbit IgG fragments (c-Ab-R) in PBS. The c-Ab-R-immobilized surface was used to detect rabbit IgG (Ag-R) by exposure to the solution of Ag-R.

Li *et al.* modified a GCE by dropping onto its surface a silver nanoparticles decorated multi-walled carbon nanotubes composite (Ag_{NP}/MWNT) [61]. The composite was characterized by TEM and XPS. TEM allowed estimating the average size of Ag_{NP}. The presence of Ag_{NP} along the MWNT network was confirmed by XPS. The detail scan of the Ag $3d_{5/2}/3d_{3/2}$ doublet (368.2 eV/374.2 eV) confirmed the presence of Ag(0) in the composite. Cyclic voltammograms were recorded at bare GCE, MWNT/GCE and Ag_{NP}/MWCNT/GCE in the absence and presence of bromate in neutral PBS. CV results evidenced a strong catalytic activity of Ag_{NP}/MWNT/GCE towards the electrochemical reduction of bromate at a relatively low overpotential. The reduction was irreversible and diffusion controlled. The performances of the CME towards bromate reduction were confirmed by chronoamperometric calibrations.

Chatchai *et al.* studied the photocatalytic (PC) and photoelectrocatalytic (PEC) properties of $WO_3/BiVO_4$ photo-anodes for organic dye degradation under visible light irradiation [62]. The performances of the photo-anodes were evaluated by monitoring the percent degradation of methylene blue (MB), as a dye sample, with UV–Vis spectroscopy. To study the charge transfer rate improvement, a Cu_2O electrode was employed as a photocathode. Both materials were supported by F-doped tin oxide (FTO) conducting electrodes. The characterization of the electrodes was made by SEM, XPS and XRD, before and after their modification by potentiostatic deposition of Ag nanoparticles. The XP Ag $3d_{5/2}$ spectrum on the surface of the cathode (368.1 eV) confirmed the presence

of Ag(0). The Ag 3d spectrum of the film present onto the $WO_3/BiVO_4$ anode was shifted by 0.2 eV (367.9 eV). UV-Vis measurements allowed testing the performance of the electrodes by monitoring the percent degradation of MB under irradiation by a Xenon lamp. The mechanism of MB degradation, studied by monitoring the CO_2 production during the photoelectrocatalytic process, confirmed that the final product was CO_2, as suggested by the absence of other absorption peaks in the spectra. The best catalytic performances for MB degradation were exhibited by the $WO_3/BiVO_4$/FTO anode under PEC conditions and by the Cu_2O-Ag_{NP} under both PC and PEC conditions.

Hu *et al.* prepared a nonenzymatic glucose sensor based on ITO electrodes modified by nickel ion implantation [63]. The morphology of nickel nanoparticles was characterized by SEM. After ion implantation, the rugged grains observed on the bare ITO electrode surface disappeared, likely because of the sputtering effect of implanted nickel ions. The surface of the ITO electrodes before and after the implantation of Ni nanoparticles (Ni_{NP}) was characterized by XPS. The Ni $2p_{3/2}/2p_{1/2}$ doublet (852.7 eV/870.0 eV; SoS 17.3 eV), observed only after the modification, was assigned to Ni(0). The electrochemical behavior of the sensor was investigated by CV. After CV scanning, a pair of redox peaks could be evidenced corresponding to Ni(II)/Ni(III) redox couple. This finding was also evidenced by XPS because, after CV scanning, the Ni 2p region evidenced the presence of an additional doublet (855.8 eV/857.1 eV) assigned to $Ni(OH)_2$ and NiOOH species. CV and CA were used to explore the electrochemical oxidation of glucose at the CME. The good electrocatalytic properties of Ni_{NP}/ITO electrodes toward glucose oxidation suggested their suitability as nonenzymatic glucose sensors.

Lee, Malhotra *et al.* described a method to deposit Sm_2O_3 nanorods (Sm_2O_{3NR}) onto an ITO glass substrate via an electrophoretical deposition technique [64]. The Sm_2O_{3NR} was characterized by XRD, AFM, TEM, FTIR and XPS. The survey XPS scan evidenced only the presence of carbon, oxygen and samarium. The Sm 3d region was fitted by a $3d_{5/2}/3d_{3/2}$ doublet (1083.1 eV/1110.2 eV), assigned to Sm^{3+}. A broad, low intensity peak centered at ~1096 eV, assigned to Sm^{2+} traces, suggested a small amount of oxygen vacancies, allowing charge transferring. The Sm_2O_{3NR}/ITO electrode was used for the co-immobilization of monoclonal antibodies of aflatoxin B1 (Ab-AFB1) and bovine serum albumin (BSA) via electrostatic interactions. The electrochemical performances of the resulting BSA/Ab-AFB1/Sm_2O_{3NR}/ITO immunoelectrode, characterized by CV, confirmed that the Sm_2O_{3NR}/ITO electrode was capable of immobilizing Ab-AFB1. Amperometric measurements suggested that antibodies bioconjugated with Sm_2O_{3NR} were thermally stable. The response of the CME to aflatoxin B1 was tested in pH 6.0 PBS. The sensing performances of the immunoelectrode suggested that it could represent a suitable platform for the application of rare earth metal oxide materials in clinical diagnostics, antibody screening and proteomics research.

Tanwar *et al.* developed a one-step synthesis of two electroactive nanocomposites (nComps), Au-polyaniline-4-sulfocalix[4]arene (Au-PANI-Calix) and Au-polyaniline S-Naproxen (Au-PANI-Nap) [65]. The nComps were characterized by TEM, UV–Vis, FTIR, Raman, dynamic light scattering, XRD, EDX and XPS. XRD analyses supported the presence of doped PANI and Au(0) nanoparticles in the nComps. XPS survey scans showed the presence of C, N, O, S and Au in both nanocomposites. In particular, the Au $4f_{7/2}/4f_{5/2}$ doublet (83.5 eV/87.2 eV) and the relevant SoS (3.70 eV) confirmed the presence of elemental gold. Results from XPS, IR and XRD confirmed the doping and successful synthesis of the nComps. DMF solutions of the Au-PANI-Calix and Au-PANI-Nap composites were casted on screen-printed electrodes (SPEs) and the electrochemical behavior of the two resulting CMEs was

investigated in PBS by CV by using the $Fe(CN)_6^{3-/4-}$ redox couple. The Au-PANI-Calix modified SPE was applied to the interference-free SWV detection of Cu^{2+} while that based on Au-PANI-Nap was applied to the detection of hydrogen peroxide in N_2-saturated PBS.

Hu *et al.* developed a nonenzymatic glucose sensor obtained by depositing gold nanoparticles on an indium tin oxide electrode (Au_{NP}/ITO) via an ion implantation technique [66]. The CME was characterized by AFM, XPS and CV. The presence of Au_{NP} on the substrate was confirmed by XPS, as verified by the BEs of the Au $4f_{7/2}/4f_{5/2}$ doublet (84.2 eV/87.9 eV). The quantitative analysis of AFM images evidenced a change in the root mean squared roughness (Rrms) after ion implantation, thus confirming the creation of a new interface. The electroactivity of the Au_{NP}/ITO electrode towards glucose was explored by CV in alkaline aqueous solution. The results of CV tests at different scan rates allowed proving that the glucose electroxidation was a diffusion-controlled process. Moreover, CV allowed verifying that that ascorbic acid and 4-acetamidophenol had negligible effects on the oxidation of glucose. The Au_{NP}/ITO electrode was applied to the glucose detection in glucose injection samples.

Koçak and Aslışen electrochemically deposited gold nanoparticles onto the surface of a GCE previously modified by CNT and poly(bromocresol purple) p(BCP) [67]. The Au_{NP}/p(BCP)/CNT/GCE was characterized by EIS, SEM/EDX and XPS techniques. In particular, SEM images of the CME showed round-shaped, homogeneously dispersed Au_{NP} adhering to the p(BCP)/CNT/GC electrode surface. XP wide scans showed the presence of Na 1s peak besides the more intense C 1s, O 1s and Au 4f signal. The Au $4f_{7/2}/4f_{5/2}$ doublet (84.6 eV/88.3 eV) was assigned to Au(0). EIS results confirmed the successful electrochemical synthesis of the p(BCP)/CNT/GCE and Au_{NP}/p(BCP)/CNT/GCE. CV and amperometry were used to study the electrocatalytic oxidation of hydrazine in pH 10 PBS at bare GCE, CNT/GCE, p(BCP)/CNT/GCE and Au_{NP}/ p(BCP)/CNT/GCE. The redox reactions at all electrodes were diffusion controlled. The best catalytic activity was displayed by the Au_{NP}/p(BCP)/CNT/GCE.

Santhanalakshmi *et al.* prepared a gold nanoseed (Au_{NS}) mediated growth of bullet-like gold–zinc oxide (Au–ZnO) heterodimer nanoparticles (HNP) [68]. The heterojunction effect of the Au–ZnO_{HNP} was studied using UV-Vis, XPS, HRTEM and EIS. HRTEM images confirmed the formation of individual Au-ZnO bullet-like HNP. XPS was used to explore the surface chemical composition of Au_{NS}, Au–ZnO_{HNP} and ZnO_{NP}. In particular, the differences in BE of the Au $4f_{7/2}$ peak of Au_{NS} (83.6 eV), typical of Au(0), from that of the Au–ZnO heterodimer was interpreted as due to the strong interaction between the Au_{NS} and bullet-like ZnO_{NP}. The Zn $3p_{3/2}/3p_{1/2}$ doublet of Au–ZnO_{HNP} (88.62 eV/91.1 eV) was partially overlapped with the Au 4f region. The Zn $2p_{3/2}/2p_{1/2}$ doublet (1021.9 eV/1044.8 eV; SoS 22.90 eV) was assigned to Zn(II). The XPS analysis was completed by C 1s and O 1s curve fittings. The electrochemical behavior of bare GC, MWCNT/GC, Au/MWCNT/GC and Au–ZnO_{HNP}/MWCNT/GC modified electrodes was characterized by CV experiments in the presence of $K_4(Fe(CN)_6)$. The Au–ZnO_{HNP}/MWCNT/GCE was applied to the nonenzymatic determination of glucose. CV results proved that glucose oxidation at the CME was a diffusion-controlled process. Amperometric measurements confirmed the appreciable performances of the Au-ZnO modified electrode. The sensor was applied to the determination of glucose in human blood serum samples.

Proust, Combellas *et al.* attached Keggin-type polyoxometallates (POM) to gold or glassy carbon surfaces by chemical or electrochemical grafting from POM-N_2^+ or by chemical grafting via peptidic coupling from POM-NH_2 [69]. The effective attachment was verified by electrochemical, ellipsometric, XPS, and FT-IRRAS techniques. The survey XP spectrum of POM-Au sample evidenced the presence

of Au, C, O and W. C 1s and W 4f regions were carefully fitted by reporting BEs, FWHM and SoSs data. The W 4f region, in particular, was decomposed into two 4f doublets: the highest $4f_{7/2}$ peak (36.35 eV) was assigned to the grafted POM on the gold surface, the lowest $4f_{7/2}$ peak (35.05 eV) was explained by some radiation damage. FT IRRAS was used to compare the results of the different grafting methods and to prove that the modified layer was stable over 1 month period. The grafting on GC electrodes was found more stable toward electrochemical polarization than on Au electrodes. The redox behavior of the grafted POM surfaces was evaluated by CV and SWV. An estimate of the overall averaged surface coverage was obtained from the variation of the integrated SWV signal with the SWV frequency. Depending on the experimental conditions, the grafting was controlled from 0.1 to 5 monolayers.

Kaim *et al.* synthesized a series of thioacetyl-functionalized fullerene-C60 derivatives by using the Prato reaction of fullerene-C60 with six different 4-(S-acetylthioalkyl)benzaldehydes [70]. The structure of the synthesized compounds was characterized by FTIR, ^{1}H NMR, AFM, EIS and ESI-MS techniques. LUMO–HOMO energy gap values obtained by computational calculations allowed estimating the yield of the Prato reaction. Functionalized fullerenes were deposited onto gold electrodes via self-assembly following an *in situ* deprotection procedure, which transformed thioacetyl-functionalized compounds into their thiolated derivatives. The solvent dependent barrier properties of the films were studied by CV, DPV and EIS. In particular, the sequence of four DPV peaks characteristic of the extended p-electron system of fullerene moieties, resulted cathodically shifted at the thioacetyl derivatives. This was explained by the presence of the substituent containing an electron-donating moiety (the aromatic ring). The XPS survey scan of the Au-modified electrodes evidenced the presence of gold, sulfur, nitrogen, oxygen and carbon. The Au $4f_{7/2}/4f_{5/2}$ doublet (83.6/87.2 eV) was assigned to Au(0). The N1s region was fitted by three peaks assigned to cyanide (397.5 eV), pyrrolidine ring attached to the fullerene (399.4 eV) and quaternary ammonium nitrogen (403.1 eV). Together with the results of the S 2p region fitting and AFM measurements, these findings confirmed the stable modification of the Au substrate by a three dimensional film of worm-like fullerene aggregates.

3.3. Multielement Analysis

Gong, Zhang, Hu *et al.* performed a SEM/XPS/CV/DPV study aimed at preparing a GCE modified by bimetallic Au-Pt inorganic/organic nanofibers [71]. 3,3',5,5' -tetramethylbenzidine (TMB) based organic nanofibers (Org_{NF}) were first doped with Pt(II) through a wet-chemical process. Subsequently, Au nanoparticles (Au_{NP}) were electrodeposited by CV scanning onto the 3D interlaced network of the TMB-based OrgNF. This led to the formation of bimetallic Au-Pt_{NP}/Org_{NF} hybrid nanostructures. SEM images showed that the Au-Pt_{NP} were homogenously distributed in the nanofibers matrix. GCEs modified by the Au-Pt_{NP}/Org_{NF} were characterized by XPS. Detail scans of the Au $4f_{7/2}/4f_{5/2}$ doublet (84.0/87.7 eV) confirmed the presence of Au(0). The Pt $4f_{7/2}/4f_{5/2}$ region was fitted by two doublets. The first (71.5/75.2 eV) was assigned to Pt(II), while the second (72.5/75.5 eV) was assigned to Pt(0). This proved that a part of Pt(II) ions in the nanofibers was reduced to Pt(0) during the electrodeposition of Au_{NP}. CV tests, performed by using the $Fe(CN)_6^{3-}$ probe, allowed confirming that the Au-Pt_{NP}/Org_{NF}/GCE sensor had a three-dimensional porous nanoarchitecture in which the bimetallic Au-Pt_{NP} served as a metal microelectrodes ensemble homogenously distributed in the matrix of

interlaced organic NFs. The CME was successfully applied to the DPV stripping assay of Hg(II) in tap and river water. The bimetallic hybrid nanomaterial could be attractive to detect toxic heavy metal ions.

Botelho do Rego *et al.* performed a CV/XPS investigation of the incorporation of $Fe(CN)_6^{3-}$ in poly(3,4-ethylene-dioxythiophene) (PEDOT) films [72]. The electropolymerization was performed by potential cycling on a platinum disk electrode dipped in a tetrabutylammonium hexafluorophosphate ($TBAPF_6$)-acetonitrile solution containing 3,4-ethylene-dioxythiophene (EDOT). PEDOT films were characterized by CV and XPS before and after the incorporation of $Fe(CN)_6^{3-}$. After the incorporation, the electrochemical behavior of the polymer evidenced the two peaks corresponding to the redox couple Fe(II)/Fe(III). The C 1s, O 1s, N 1s, S 2p and F 2p regions were analyzed by XPS. In particular, the tails of the C 1s, O 1s and S 2p regions at higher binding energies were ascribed to the existence of zones of different conductivity resulting from X-ray irradiation and differential charge accumulation in the surface films. The BE of the Fe $2p_{3/2}$ peak (709.8 ± 0.2 eV) of PEDOT/$Fe(CN)_6^{3-}$ modified electrodes and the relevant spin-orbit splitting of the Fe 2p region confirmed that the main form of iron in the film was Fe^{3+}.

Kumar and Swetha performed a CV/DPV/TEM/UV-Vis/XPS study aimed at preparing a $Ru(DMSO)_4Cl_2$ nano-aggregated NA membrane modified GCE ({H_2O-Cl-RuDMSO–Cl–H_2O}-NA/GCE) [73]. It was found that $Ru(DMSO)_4Cl_2$dissolves within the water rich hydrophilic micro-channels of membrane, being electrostatically stabilized as $[Ru(II)Cl_x(DMSO)_y\text{-}(H_2O)_{4-(x+y)}]^{n+}$. The electrochemical behavior of GC, GC-NA and {H_2O-Cl-RuDMSO–Cl–H_2O}-NA/GC electrodes was compared in neutral PBS containing $Fe(CN)_6^{3-}$. No redox reaction could be observed at the GC-NA electrode. On the contrary, at GC and {H_2O-Cl-RuDMSO–Cl–H_2O}-NA/GC electrodes the redox system showed a well-defined redox couple. These observations suggested that $Ru(DMSO)_4Cl_2$-incorporated NA membranes behaved as a perfect metal like electronic conductor. XPS, solution and solid-state UV-Vis experiments were performed on using ITO in place of GCE. XPS survey spectrum of the ITO modified electrode showed peaks related to Ru, S, Cl and O species. The Ru $3d_{5/2}$ peak (285.4 eV) was assigned to Ru(II), while the S 2p region was fitted by three species of sulfur, involved in bonded DMSO (166.5 eV), free sulfonic acid (167.6 eV) and unbounded DMSO (164.8 eV). Together with the results of details spectra relevant to the Cl 2p and O 1s regions, these findings further supported the stabilization of the $[Ru(II)Cl_x(DMSO)_y\text{-}(H_2O)_{4-(x+y)}]^{n+}$ complex by the sulfonic sites of Nafion®. The CME was proposed as a sensitive and separation-less electrochemical sensor for the DPV analysis of uric acid, xanthine and hypoxanthine in physiological solutions.

Chen *et al.* prepared a highly sensitive H_2O_2 sensor by electrochemical deposition of zinc oxide nanorod (ZnO_{NR}) arrays on an ITO substrate [74]. ZnO_{NR} arrays were deposited on ITO by constant-current electrochemical deposition (ECD). The photocurrent of ZnO_{NR} modified electrode was tested before and after sintering at 400 °C by an electro-optical testing device. Sintering improved the anodic photocurrent stability and intensity of the sensor. The CME was characterized by XRD, SEM and XPS. XPS survey scans of the ZnO_{NR} array evidenced the presence of peaks assigned to C 1s (284.6 eV), O 1s (530.22 eV) and Zn $2p_{3/2}$ (1021.2 eV) regions and to the Zn LMM (498.02 eV) Auger region. The presence of carbon was ascribed to ambient contamination. The high-resolution Zn $2p_{3/2}$ region, symmetrically centered at 1020.7 eV, confirmed the presence of ZnO on the sensor surface. The O 1s region was fitted by two components, assigned to Zn–O (529.6 eV) and to O–H groups of adsorbed water molecules (531.3 eV). After treatment with high H_2O_2 concentrations, the surface film showed

only one peak of O1s (530.94 eV). This BE value is close to that of non-lattice oxygen (531.3 eV) and indicated that H_2O_2 could remove lattice oxygen from ZnO_{NR} surface releasing oxygen. The proposed sensor proved very sensitive for detecting H_2O_2, the product of the reactions catalyzed by a large number of oxidase enzymes.

Bartlett *et al.* prepared some modified GC electrodes suitable as support for the immobilization of the laccase enzyme *Trametes hirsuta* (ThL) [75]. Six surface modifications were tested by attaching three different linkers and two terminal groups containing either anthracene or anthraquinone moieties. The surface modifications allowed the binding of ThL and provided an electrical contact between the underlying electrode and the enzyme active site. The CMEs were characterized by EIS in a $Fe(CN)_6^{3-/4-}$ containing solution. These results suggested the presence of a dense layer of enzyme adsorbed at the electrode surface. This finding was also confirmed by XPS. The C 1s region of the ThL-modified electrodes was fitted by peaks assigned to aliphatic carbon atoms, C=O (288.6 eV) and C–N or C–OX (286.6 eV) groups. Compared to those of the enzyme free surfaces, the N 1s and O 1s peak areas significantly increased after ThL immobilization. The results of the analysis of the C 1s, O 1s and N 1s regions allowed estimating the surface atomic percent of all electrodes. The activity of the sensor was tested by CV. The combination of short linkers with anthraquinone gave the best results for the direct electron transfer to the enzyme active center. The sensors were proposed as a good starting point towards development of improved enzyme electrodes.

Wang *et al.* performed a XRD, XPS, TEM, FT-IR and CV study aimed at developing a GCE modified by a nanocomposite consisting in titanate nanotubes (TNT) decorated by Prussian blue and Nafion® (NA/PB/TNT/GCE) [76]. XPS survey scans of pure TNT evidenced the presence peaks attributable to Ti 2p (459.6 eV), O 1s (531.6 eV) and C 1s (285.6 eV) regions. Additional peaks corresponding to Fe 2p (709.6 eV), N 1s (398.6 eV) and K 2p (295.6 eV) confirmed the presence of PB in the PB-TNT nanocomposite. The Fe $2p_{3/2}/2p_{1/2}$ doublets of PB-TNTs were assigned to Fe(III) (712.9 eV/721.3 eV) and to Fe(II) (708.3 eV). Together with XRD results, these findings indicated that $Fe_4[Fe(CN)_6]_3$ and a few $KFe[Fe(CN)_6]$ were present on the TNTs surface. The electrochemical performances of the NA/PB-TNT/GCE, tested by CV in the presence/absence of H_2O_2, confirmed the appreciable electrocatalytic activity of the sensor towards the reduction of hydrogen peroxide, and that it could serve as an amperometric sensor for H_2O_2 detection.

Jia, Dong *et al.* performed a CV/SEM/XRD/XPS study aimed at preparing a Pt nanoparticles (Pt_{NP}) decorated TiO_2 nanotubes (TiO_{2NT}/Pt_{NP}) modified electrode suitable for methanol oxidation reaction (MOR) [77]. The TiO_{2NT}/Pt_{NP} electrode was prepared by electrodepositing Pt_{NP} on the TiO_{2NT} support. The surface of the CME was characterized by XPS. The Ti $2p_{3/2}/2p_{1/2}$ doublet (458.7/464.1 eV) was assigned to TiO_2. The O 1s peak (529.9 eV) was assigned to bulk oxygen bonded to titanium. The Pt $4f_{7/2}/4f_{5/2}$ doublet (70.5/74.1 eV) was assigned to Pt(0). These findings indicated that Pt was successfully deposited on TiO_{2NT}. CV experiments allowed evidencing the excellent electrocatalytic activity of the TiO_{2NT}/Pt_{NP} electrode toward MOR in alkaline electrolytes without UV irradiation. This finding was interpreted on the basis of the synergistic effect between Pt_{NP} and TiO_{2NT} on CO oxidation, and of the ordered architecture of TiO_{2NT}, which can provide a unidirectional electronic channel and reduce the grain boundaries.

Adriaens *et al.* described the formation of a supramolecular self-assembled monolayer of polymeric copper-phthalocyanine (poly(CuPc)SAM) onto a gold substrate [78]. The study was performed by

CV/EIS/Raman/AFM/XPS techniques. Raman and XP spectra indicated the formation of a monolayer film of poly(CuPc) on the Au surface by evidencing characteristic peaks of CuPc in their spectra. Detail scan of the Cu $2p_{3/2}$ peak evidenced the presence of Cu(I) and Cu(II) states: see Figure 5.

The N1s region in the same Figure was fitted by a peak assigned to nitrogen atoms of the polymeric nature of the molecules (399 eV) and a small peak (401 eV) probably attributable to the presence of adsorbed molecular nitrogen or free cyano groups at the periphery. The poly(CuPc)SAM/Au electrode was characterized by cyclic voltammetry to study the redox behavior of the modified surface. CV and EIS findings relevant to the redox-active self-assembled monolayer revealed a reversible electrochemistry in aqueous solution, with an enhanced electron-transfer rate. Poly(CuPc) greatly improved the electronic communication between gold electrode surface and solution. The poly(CuPc)SAM/Au electrode exhibited a gainful electrocatalytic response toward the reduction of H_2O_2 in pH 7.0 PBS.

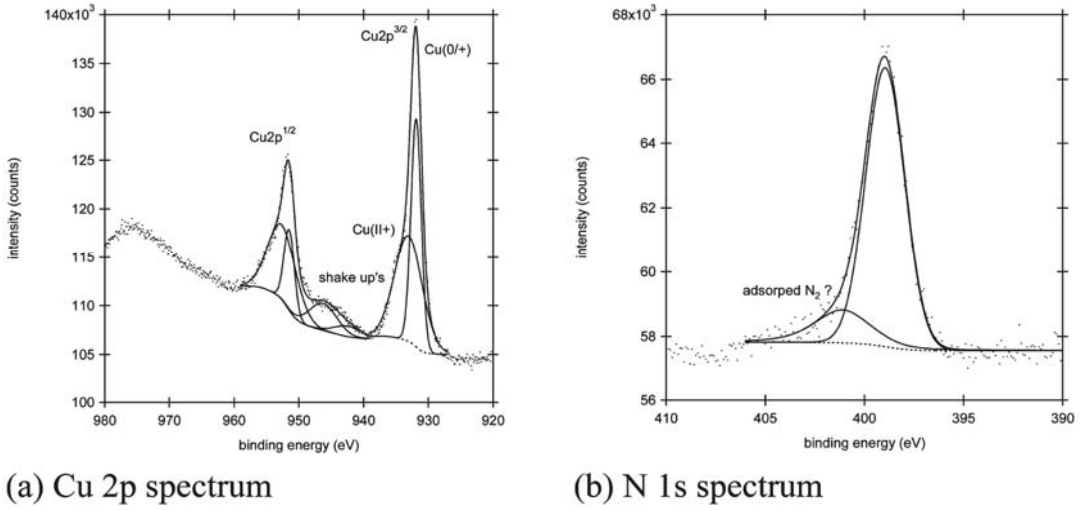

Figure 5. X-ray photoelectron spectra of (**a**) Cu 2p and (**b**) N 1s regions of a monolayer of poly(CuPc)SAM on gold [78]. Reprinted with permission from K. S. Lokesh, K. De Wael, A. Adriaens, Self-Assembled Supramolecular Array of Polymeric Phthalocyanine on Gold for the Determination of Hydrogen Peroxide, *Langmuir*, **2010**, *26* 17665–17673, doi:10.1021/la102740s. Copyright (2010) American Chemical Society.

Ghilane, Randriamahazaka *et al.* performed a CV/AFM/FTIR/XPS study of the electrochemical reduction of 4-nitrophenyl diazonium (NPD) at gold and carbon electrodes in three room temperature ionic liquids (RTIL) with different viscosities [79]. In all investigated ionic liquids, the reduction of NPD led to the attachment of 4-nitrophenyl diazonium layers onto the carbon electrode surface. IR and CV investigations of the modified electrodes showed a decrease of the amount of the attached molecules on increasing the viscosity of the grafting media. XPS allowed monitoring the attenuation of the Au 4f signal after the electrochemical reduction of NPD, thus confirming the covering of the gold substrate surface. Moreover, FT-IR and XPS data were consistent with the presence of nitrophenyl groups strongly attached onto gold electrode, independently on the viscosity of the grafting media. It could be concluded that using RTIL as grafting media allowed modulating the quantity of the attached layer and making a thinner and/or less dense layer in comparison with classical solvents.

Cabrera *et al.* described the modification of a palladium electrode by a self-assembled monolayer of L-cysteine [80]. The CME was characterized by CV, EIS, FTIR and XPS. FTIR and XPS techniques showed that L-cysteine was adsorbed on the Pd surface through the sulfur atom, while leaving the free carboxylic acid and amino groups in the surface for conjugating biomolecules. XPS characterization involved the acquisition of the Pd 3d, C 1s and S 2p regions. In particular, detail scans of the S 2p region of the CME evidenced two doublets (SoS: 1.18 eV). The relevant S $2p_{3/2}$ peaks were assigned to the thiolate formation on the surface through S–Pd bonds (162.1 eV) and to sulfonic groups of cysteic acid (166.9 eV), thus suggesting that $–OOCNH_2CHCH_2S–Pd$ was the adsorbed cysteine monolayer. The electron transfer reaction of L-cysteine modified Pd electrode was probed by CV and EIS in $Fe(CN)_6^{3-/4-}$ containing solutions. The CV measurements at bare and modified Pd electrodes revealed a quasi-reversible voltammogram of the redox probe, indicating the promotion of electron transfer between the redox couple and palladium electrode. Accordingly, EIS results at the CME were consistent with an electron transfer resistance lower than at bare Pd electrodes.

Lee, Kim *et al.* developed an estrogen-sensing electrode for the EIS detection of estrogen bindings to estrogen receptors covalently bonded to the electrode [81]. The sensor was prepared by modifying a gold electrode with 3-mercaptopropionic acid (MPA). The carboxylic groups of the MPA/Au electrode were activated by contact with a solution of 3-(3-dimethylaminopropyl)-1-ethylcarbodiimide hydrochloride/N-hydroxysuccinimide (EDC/NHS) in a PBS. Dipping the EDC-NHS/MPA/Au in a solution of estrogen-receptor α allowed a suitable covalent bonding to the receptor. XPS was used to monitor the extent of each reaction step. The S $2p_{3/2}$ peak of the MPA/Au electrode was fitted by two components, the first (162.1 eV) was attributed to S-Au bonds, the second (163.5 eV) to non-covalently adsorbed free thiol groups on the Au electrode. In the C 1s region, the peak at 288.7 eV proved the presence of carboxyl group of the MPA monolayer. The MPA modification with EDC and NHS was also monitored by acquiring the N 1s region. The two peaks at 399.7 and 400.7 eV were assigned to secondary amine and imine of EDC and, respectively, to the protonated tertiary amine of EDC. The detection of estrogen hormone was evidenced by the observed EIS impedance change at the receptor-modified electrode in the presence of the 10^{-6} M concentration of estrogen hormone in PBS buffer solution.

Brunetti and Desimoni performed a CV/XPS investigation about the electropolymerization of 8-hydroxyquinoline-5-sulfonic acid (HQSA) at glassy carbon electrodes in hydrochloric acid solutions [82]. For a better understanding of the complex surface functionalization of the modified electrode, another GCE (ox-GCE) was also prepared by using the same electropolymerization parameters but in absence of HQSA. It is in fact known that potential cycling treatment can led to oxygenated functionalities on carbonaceous surfaces. Survey and detail XPS scans were performed for characterizing the two CMEs. The S 2ppeak (168.2 eV), assigned to sulfonic groups, confirmed the presence of HQSA on the HQSA/GCE surface. As expected, the S 2p region was absent on the surface of the ox-GCE. A deeper interpretation of the different XP regions of the two CMEs was postponed to a more exhaustive XPS investigation (described below, after reference [90]). CV measurements allowed comparing the electrochemical behavior of HQSA-GC, ox-GC and bare GC electrodes. The HQSA/GCE showed improved electrochemical performances with respect to those of the other two electrodes. The attractive features of the HQSA/GCE were evidenced by determining species of alimentary and pharmaceutical interest such as dopamine, theophylline and tartrazine.

Ganesh *et al.* prepared copper-hexacyanoferrate (CuHCF) and nickel-hexacyanoferrate (NiHCF) modified ITO electrodes suitable for the electrocatalytic oxidation of alcohols in alkaline medium [83]. At first, CuHCF and NiHCF (in general, metal hexacyanoferrate, MHCF) were potentiodinamically deposited on ITO electrodes. Then, both electrodes were cycled in aqueous NaOH solutions to convert MHCF films to their corresponding $M(OH)_2$ moieties. Both MHCF and $M(OH)_2$ films were characterized by SEM-EDAX and XPS. In the case of MHCF films, detail scans evidenced the presence of Ni $2p_{3/2}$ (852 eV) or Cu $2p_{3/2}$ (931.7 eV) and Fe $2p_{3/2}$ (703 eV). Only Ni 2p and Cu 2p doublets were unaltered by the potential cycling conversion to $M(OH)_2$. The Fe 2p doublet progressively decreased up to disappear with the number of cycle, revealing the cleavage of Fe–CN–Ni/Cu bond followed by dissolution of iron as hydroxide species. The electroxidation ability of the two CMEs was investigated by CV. The results proved that metal hydroxide modified electrodes display good catalytic performances and stabilities for direct methanol or alcohols oxidation, along with low CO poisoning effect.

Millner *et al.* prepared organic thiol-modified glassy carbon electrodes (RSH/GCE) by potentiostatic electroxidation in tetrabutylammonium hydroxide (Bu_4NOH)/acetonitrile [84]. Adding Bu_4NOH, a strong deprotonating agent, allowed an easier oxidation/deposition of thiols onto the carbon surface. The tested thiols were n-octanethiol, 3-(nitrobenzyl)mercaptan (NBM), cysteamine and N-acetylcysteamine. The CMEs were characterized by CV and XPS. The surface composition of NBM/GCE before and after modification was monitored by following the C 1s, N 1s, O 1s and S 2p photoelectron spectra. The disappearance of N 1s signal assigned to the $C–NO_2$ peak (404 eV), the increase of the N 1s signal assigned to $C–NH_2$/NHOH/NO peak (400 eV) and the unchanged S 2p signal (164 eV) proved that the electrochemical reduction of nitrophenyl groups deposited during NBM oxidation was complete. NBM, the model thiol used for exploring the possibility of thiols oxidation, proved capable of grafting the carbon surface. In addition, the electrochemical results confirmed the stable binding of thiols and that the surface modification occurred independently from $RS^{\bullet}$ radicals formation and was explained by nucleophilic addition of deprotonated thiols to the carbon surface.

Li, Sun *et al.* performed a CV/DPV/XPS/SEM/EDS and UV-Vis-NIR study about the electrochemical properties of three fullerene-modified electrodes in aqueous solutions [85]. This was allowed by drop-casting toluene solutions of the three isomers (C_{84}-D_2(IV), C_{84}-Cs(a), and C_{84}-C_2(IV)) onto GC electrodes. Only the C_{84}-C_2(IV)/GC modified electrode showed a couple of redox peaks. CV experiments allowed proving that those peaks were relevant to reduction/oxidation processes of the C_{84}-C_2(IV) film. CV measurements at the CME in aqueous solutions of different salts proved that cations, not anions, played an important role in the electrochemistry of the modified electrode. XPS measurements were performed in the presence of KCl to prove that the K^+ ions were incorporated into the C_2(IV) films upon reduction. The C 1s peak of the reduced film was fitted by components assigned to negatively charged carbon atoms (283.4 ± 0.2 eV), indicating the reduction of C_2(IV), to neutral carbon atoms (284.8 ± 0.2 eV) and to positively charged carbon atoms (286.5 ± 0.2 eV). These findings, together with the appearance of the K 2p photoelectron signal, allowed confirming that K^+ ions were incorporated in the C_{84}-C_2(IV) surface film upon reduction. Furthermore, interaction between C_2(IV) and guanine was investigated by DPV, UV-Vis-NIR and XPS. The results evidenced that guanine and C_2(IV) formed a charge-transfer complex due to their interaction, so that the reduction of C_2(IV) was blocked in the complex. The complex formation was also confirmed by the evolution of the N 1s signal

before and after the interaction. Thus, the reoxidation peak current of C_2(IV) decreased with the increase of the guanine concentration.

S-H. Cheng *et al.* electrodeposited on a screen-printed carbon electrode (SPCE) a hybrid composite consisting of a thin layer of the conducting poly(3,4-ethylenedioxythiophene) (PEDOT) polymer plus gold nanoparticles [86]. The nanocomposite was characterized by UV/TEM/CV/DPV/FIA/XPS techniques. The successful modification of the SPCE was checked by acquiring the C 1s, S 2p and Au 4f XPS regions. Assigning the S $2p_{3/2}$ peak (162.9 eV) to sulfur atoms in the thiophene ring, and the Au $4f_{7/2}/4f_{5/2}$ doublet (82.8/86.5 eV) to Au(0), allowed confirming the successful modification by Au_{NP}. The electrochemical applications of the CME were explored by CV in deaerated cysteine-containing buffer solutions. The results showed that the PEDOT-Au_{NP}/SPCE was characterized by a favorable electrocatalytic activity towards the oxidation of cysteine in the 2.0–8.0 pH range. The CME allowed the separation of cysteine and glutathione oxidation peaks. Cysteine could be determined by DPV in the presence of a high concentration of glutathione.

Kannan and John described a simple polymerization strategy for preparing Au_{NP}-conducting polymer films on GC and ITO surfaces by using 5-amino-2-mercapto-1,3,4-thiadiazole (AMT) capped gold nanoparticles (AMT-Au_{NP}) [87]. The study was performed by CV/EIS/AFM/FTIR/XPS techniques. AFM results revealed the homogeneous distribution of Au_{NP} in the modified film. The Au 4f XPS region allowed proving the presence in the modified film of Au(0). The N 1s region was fitted by three peaks assigned to imine nitrogen =NH (396.7 eV), secondary amine nitrogen –NH– (399.6 eV) and positively charged nitrogen $–N^+H–$ (403.3 eV), thus confirming that the electropolymerization proceeded through the oxidation of $–NH_2$ groups present on the periphery of the AMT-Au_{NP}. The CME electrocatalytic performances were tested by studying the electroreduction of oxygen at pH 7.2. The AMT-Au_{NP} film showed an excellent electrocatalytic activity towards the reduction of oxygen at physiological pH, suggesting the possibility of potential applications in energy storage systems and electrochemical sensors.

Ma, Huang *et al.* performed a CV/SEM/TEM/FTIR/UV-Vis/XPS study aimed at developing a one-step electrochemical synthesis of graphene/PANI composite film onto GCE and ITO electrodes [88]. XPS was used to characterize the chemical status of the surface film by examining the C 1s, O 1s, N 1s and S 2p regions. The N 1s region was fitted by three different peaks assigned to benzenoid amine (399.4 eV), quinoid amine (398.8 eV) and nitrogen cationic radical ($N^{+\bullet}$, 401.4 eV). The C 1s region was fitted by five components assigned to C–C (284.5 eV), C–N (285.6 eV), C–O (286.6 eV), C=O (288.2 eV) and O–C=O (290.2 eV) groups, thus proving the existence of few oxygen functionalities in the obtained graphene of graphene/PANI, which were not evidenced by FTIR. In agreement with UV-Vis data, the surface atomic S/N ratio of PANI confirmed its high doping level. The sensor was used to construct a biosensor after entrapping onto its surface horseradish peroxidase. The CME exhibited a high catalytic activity for the reduction of H_2O_2. Moreover, the graphene/PANI composite film could be directly used as supercapacitor electrode.

Shi *et al.* performed a CV/SEM/TEM/EIS/XPS study aimed at characterizing some GCEs modified by nitrogen doped multiwalled carbon nanotubes (N-MWCNT) decorated with SnO_2, CeO_2 or SnO_2+CeO_2 nanoparticles [89]. TEM images revealed that SnO_2 and CeO_2 nanoparticles were uniformly attached on the surface of the N-MWCNT. Detail XP scans of Sn $3d_{5/2}/3d_{3/2}$ doublet of the SnO_2/N-MWCNT composite (486.4 eV/494.8 eV) confirmed the presence of SnO_2. The Ce $3d_{5/2}/3d_{3/2}$

(882.8 eV/900.9 eV) detail scans of CeO_2/N-MWCNT confirmed that cerium was mainly present as Ce(IV). The N 1s region of N-MWCNT, SnO_2/N-MWCNT and CeO_2/N-MWCNT was investigated in order of studying the interaction between nitrogen atoms and metallic oxides NPs. N 1s detail scans of the three electrodes were fitted by four peaks assigned to the pyridine-like nitrogen (398.7 eV), graphite-like nitrogen (401.0 eV), molecular N_2 (404.3 eV) and nitrogen oxides adsorbed on the surface of N-MWCNT (407.0 eV). Together with the results relevant to the Sn 3d and Ce 3d regions, these findings supported the existence of strong interaction between metallic oxide NPs and nitrogen atoms. CV experiments proved that N-MWCNT-based composites, as electrode materials, show a better electrocatalytic activity for NO electroxidation than the conventional CNTs-based composites. This suggested potential applications as a sensor for NO.

Yuan, Niu *et al.* grafted poly(4-vinylpyridine) (PV4P) to multiwalled carbon nanotubes by in-situ free radical polymerization of the monomer [90]. The PV4P-g-MWCNT hybrids were loaded with phosphotungstic acid (PW). The resulting material was characterized by SEM, TEM, FTIR and XPS. SEM/TEM images showed that, after the grafting step, MWCNT were wrapped in a thick layer of PV4P. MWCNT, PV4P-g-MWCNT and PW/PV4P-g-MWCNT hybrids were characterized by XPS. The comparison of C 1s, N 1s and O 1s peaks relevant to the various hybrids samples confirmed their chemical status after each preparation step. After PV4P was grafted onto MWCNT, a new C 1s peak (286.2 eV), assigned to C–N bind of pyridine group at PV4P chains, added to those assigned to hydroxyl (286.2 eV) and carbonyl (287.2 eV) carbons. The appearance of the W 4f signal in the range from 33 to 40 eV proved the presence of PW in the PWs/PV4P-g-MWCNT hybrid. CV results obtained at a PWs/PV4P-g-MWCNT/GCE showed that its electrochemical behavior followed a four-one-electron surface-confined process of Keggin-type PWs. The electrochemical study proved that PWs/PV4P-g-MWCNT hybrids are promising candidates for NO_2^- sensors in food safety and medical diagnosis.

Desimoni *et al.* performed an XPS study aimed at characterizing the surface of glassy carbon electrodes chemically modified with 8-hydroxyquinoline-5-sulfonic acid (HQSA/GCE) [23]. The work completed a previous electrochemical investigation on the same CME [82]. Spectroscopic experiments involved acquiring survey and detailed scans of C 1s, O 1s, Si 2p, Cl 2p, N 1s, and S 2p regions of an HQSA powder standard sample as well as of GC electrodes cycled both in the presence and in the absence of HQSA. The experimental value of the binding energy of the S $2p_{3/2}$ level of HQSA-modified electrodes (167.6 eV) was found equal to that of the HQSA standard powder, thus confirming that HQSA molecules were adsorbed on the surface of the HQSA/GC electrodes (see Figure 6) and that sulfur maintained its chemical structure and properties. The C 1s spectrum of the CME was fitted by five peak components associated to graphitic carbon (284.5 eV), CH_x (285.0 eV), C–O (286.3 eV), C=O (287.7 eV) and O=C–OH (289.0 eV). The experimental S/N and O/S ratios estimated for the HQSA standard were slightly different from the theoretical ones, suggesting a limited degradation of the powder under X-ray irradiation.

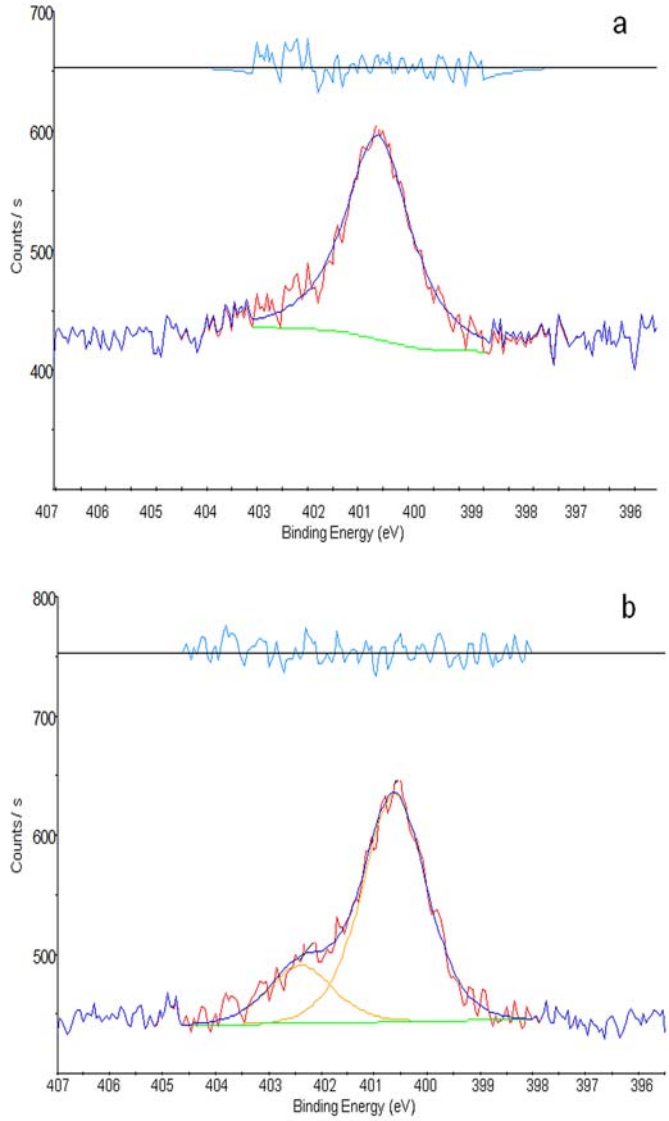

Figure 6. Comparison of fit of the S2p regions: (**a**) 8-hydroxyquinoline-5-sulphonic acid/glassy carbon electrode (HQSA/GCE) and (**b**) HQSA powder. The plots of residuals above the fitted peaks shows the (properly expanded) differences between experimental and synthesized spectra [23].

Solak *et al.* modified a GCE with 3-aminophenylcalix[4]pyrrole (3APCP) by electro-oxidation in tetrabutylammonium-tetrafluoroborate (TBATFB)-acetonitrile solutions [91]. The presence of the modifier film onto the GCE surface was confirmed by comparing CV profiles of dopamine and ferricyanide redox probes at the bare and modified electrodes. The CME surface was characterized by RAIRS, XPS, AFM, ellipsometry and contact angle measurements. RAIRS analysis revealed that calix[4]pyrrole was bonded to the GCE surface via the etheric linkage. XPS results were acquired during potential cycling. After six cycles, the N 1s region of the CME was fitted by components assigned to pyrrole NH groups (397.2 eV), to the amine nitrogen of meso-p-aminophenyl substituent in the calix[4]pyrrole ring (400.2 eV) and to residual tetrabutylammonium (402.0 eV). The C 1s region was also fitted by three components, assigned to C–C and C–H (284.5 eV), C–O (286.4 eV) and C–N (288.7 eV) groups. The presence of F 1s signal at about 690 eV and of the low B 1s signal also confirmed the

complex formation between BF_4^- ions and the calix[4]pyrrole moieties. The stability of the 3APCP film at the GC surface *versus* the applied potential was evaluated by a series of CV voltammograms acquired in the presence of the of $Fe(CN)_6^{3-/4-}$ redox probe.

Ho *et al.* developed a template-free synthetic procedure for preparing a conducting metal-doped polymer nanocomposite [92]. The study, performed by CV/TEM/EDX/FTIR/XPS techniques, implied using PPY, $HAuCl_4$ and 4-sulfocalix[4]arene as a reductant, oxidant and dopant, respectively. TEM images showed that gold nanoparticles were uniformly distributed throughout the nanocomposite material (gold particles-encapsulated polymer). The presence of 4-sulfocalix[4]arene in the nanocomposite was confirmed by FTIR, EDX and XPS. XPS evidenced the presence of C, N, O, S and Au in the nanocomposite. The S 2p (167.5 eV) and S 2s (230 eV) regions were assigned to sulfate ions dopants of Calix-PPY and Au-Calix-PPY, while the Au $4f_{7/2}/4f_{5/2}$ doublet (83.5/87.2 eV, respectively) confirmed the presence of Au(0) on the Au-Calix-PPY nanocomposite surface. CV experiments, performed at screen-printed carbon electrodes modified by drop coating the nanocomposites, showed improved electrocatalytic properties of the CME towards the electro-oxidation of formaldehyde and glucose.

Xu *et al.* prepared a potassium-modified graphene suspension to be used in nitrite-selective sensors [93]. The suspension was characterized by CV/TEM/AFM/XPS techniques. AFM images of the thickness of graphene sheet before and after K-modification allowed concluding that the introduction of K cations and/or oxides and/or metals was assembled on a monolayer of graphene sheet. In agreement with these results, XP spectra proved that potassium, absent in graphene (GR) samples, were present on the surface of the K-modified GR. At low K-coverages, the K $2p_{3/2}/2p_{1/2}$ doublet (293.2 eV/296.0 eV) was assigned to K oxides and cations. At higher K-coverages, a second doublet (294.4 eV/297.1 eV) was evidenced and assigned to metallic K. The C 1s region was fitted by contributions of C–C and C–H bonding (284.6 eV) and of C–O, C=O and C–C=O bonding (at 285.9 eV, 287.0 eV, and 288.8 eV, respectively). The intercalation of K species changed Fermi level and charge transfer, opening the band gap of the GR. This improved the electrocatalytic activity of graphene in electrochemical systems. The suspension of K-modified GR was drop casted on the surface of GCEs. The electrochemical behavior of the K-modified-GR/GCE was explored by CV in PBS containing nitrite ions. The CME exhibited good analytical performances. Responses were unaffected by high concentrations of a series of inorganic anions, cations and saccharides. Promising performances were also assumed in biosensing, energy conversion, biomedical, and other electronic systems applications.

Yuan, Niu *et al.* anchored nickel hexacyanoferrate nanoparticles ($NiHCF_{NP}$) to multiwalled carbon nanotubes with a grafted poly(4-vinylpyridine) (PV4P) linker for electrically switched ion exchange [94]. TEM and FTIR findings confirmed the presence of highly dispersed $NiHCF_{NP}$ on the surface of the $NiHCF_{NP}$/PV4P-g-MWCNT composite. CVs experiments performed at a $NiHCF_{NP}$/PV4P-g-MWCNT/Au modified electrode evidenced its considerable capacity and stability as ion exchanger. $NiHCF_{NP}$ could be reversibly switched between reduced and oxidized states depending on the applied potential. A reversible uptake and release of Na^+, K^+ and Cs^+ cations accompanied the redox process, allowing maintaining the charge neutrality within the NiHCF matrix. XPS results acquired after the CME exposition to high concentrations of Na^+ ions confirmed its good selectivity for Cs^+ over Na^+ ions. The stronger affinity of the composite towards Cs^+ was consistent with CV data.

Li *et al.* incorporated a water-soluble ionic liquid, 1-butyl-3-methylimidazolium tetrafluoroborate ([BMIM]BF_4), into TiO_2 nanoparticles to fabricate a hybrid film modified glassy carbon electrode [95]. The modification of GCEs was performed electrochemically, by dipping the GCE in a solution containing [BMIM]BF_4 and tetrabutyltitanate. The obtained nano-TiO_{2NP}/[BMIM]BF_4/GCE was characterized by SEM and XPS. XPS survey scans evidenced the presence of C 1s, N 1s, Ti 2p, O 1s and F1s signals. The Ti 2p (~ 458 eV) and O 1s (532.9 eV) signals were assigned to the nano-TiO_2 matrix. The C 1s (~285 eV), N 1s (~401 eV) and F 1s (~684 eV) peaks were attributed to [BMIM]BF_4. XPS data allowed estimating 4.1% and 2.3% atomic percentages of F and Ti, respectively. The CME was then applied to study the electrochemical behavior of p-acetaminophen in slightly acidic PBS. CV results indicated that the TiO_{2NP}/[BMIM]BF_4 hybrid film improved the redox reactions of p-acetaminophen in aqueous medium, and that it was more efficient than TiO_{2NP}/GCE and bare GCE to surface accumulate the analyte, thus enhancing the sensor sensitivity. The sensor was successfully applied to the SWV analysis of p-acetaminophen in urine samples.

Deng *et al.* developed an amperometric uric acid biosensor based on a nanobiocomposite derived from thionine modified graphene oxide (T-GO) [96]. The T-GO composite was characterized by CV/amperometry/TEM/AFM/UV-Vis and XPS techniques. UV-Vis spectra of the T-GO suspension confirmed that thionine molecules were attached to GO. XPS allowed exploring their interactions. Survey XPS scans of T-GO evidenced the signals of C, O, N and S. The C 1s region was fitted by four peaks assigned to C–C (284.6 eV), C–O (286.7 eV), C=C (287.8 eV) and O–C=O (288.7 eV) carbons. The N 1s region was fitted by two peaks assigned to amine groups (401.8 eV) and pyridine-N-oxides (402.3 eV). The S 2p signal (169.1 eV) was assigned to S–N bond in thionine molecule. These findings confirmed the noncovalent functionalization of graphene oxide by thionine. CV and amperometric measurements proved that the composite, due to the synergistic effect between thionine and graphene oxide, exhibited excellent performances towards H_2O_2 reduction. Uricase (UOx) modified T-GO/GC electrodes were prepared by casting a UOx plus T-GO suspension onto the surface of GCEs. In the presence of oxygen, the UOx/T-GO/GCE catalyzed the oxidation of UA to allantoin, with the simultaneous production of H_2O_2. This H_2O_2 is reduced at the CME surface without interferences from other electroactive compounds present at physiological levels (glucose, ascorbic acid, noradrenalin and dopamine). The CME was applied to the analysis of UA in human blood and urine.

Abraham *et al.* performed an EIS/SEM/EDS/XPS/SIMS investigation aimed at improving the performances of high-capacity lithium-ion(+)/graphite(−) cells by modifying the $Li_{1.2}Ni_{0.15}Mn_{0.55}Co_{0.1}O_2$-based positive electrode with alumina [97]. The modification modes were (i) atomic layer deposition (ALD) of alumina and (ii) addition of nanoscale alumina powder. EIS data showed an improvement of full-cell AC impedance by ALD coatings. EDS elemental maps proved that all electrode constituents, including the binder, were covered by the alumina coating. C 1s, O 1s, F 1s and Al 2p XP spectra were acquired for monitoring the changes induced on positive electrode surfaces by the ALD process. The F1s intense peak at 687.8 eV was assigned to the PVDF binder (Solef® PVDF is a fluorinated semi-crystalline thermoplastic which is obtained by polymerizing vinylidene fluoride). The O1s peak at 529.6 eV was assigned to the $Li_{1.2}Ni_{0.15}Mn_{0.55}Co_{0.1}O_2$ substrate and the weak peak centered at 532 eV to a Li_2CO_3 impurity. Cycling produced a marked decrease of Al 2p and O 1s regions of the positive electrode. An original equation was developed for estimating the thickness of the alumina layer from XPS data. SIMS results proved that the alumina coating did not significantly alter

the initial charge/discharge cycling characteristics of the cells. The modification was aimed at enhancing the electronic conductivity within the electrode laminate, improving the surface stability of the coated materials, or providing a physical barrier capable of suppressing detrimental chemical side reactions between electrode surface and electrolyte. The overall results suggested that only very thin alumina coatings could improve the cell performances while thicker coatings worsen capacity retention.

Chen *et al.* developed an amperometric glucose biosensor based on gold/platinum hybrid functionalized zinc oxide nanorods (Pt–Au/ZnO_{NR}) and glucose oxidase (GOx)–lectin biospecific interaction [98]. The CME was obtained by modifying a GCE in sequence with a gold/platinum hybrid functionalized zinc oxide nanorods, a layer of porous gold nanocrystals (pAu) and concanavalin A (ConA). At last glucose oxidase was immobilized on the ConA/pAu/Pt–Au/ZnO_{NR}/GCE by the biospecific interaction between GOx and ConA. The Pt–Au/ZnO_{NR} composite was characterized by TEM and XPS. XP detail spectra were relevant to the O 1s, Zn 2p, Au 4f and Pt 4f regions. The Zn $2p_{3/2}/2p_{1/2}$ doublet (1021.1 eV/1044.9 eV) was assigned to ZnO. The Au $4f_{7/2}/4f_{5/2}$ (83.6 eV/87.6 eV) and the Pt $4f_{7/2}/4f_{5/2}$ (70.8 eV/74.1 eV) doublets, assigned to the formation of Pt–Au hybrid on the surface of ZnO_{NR}, confirmed the successful preparation of the Pt–Au/ZnO_{NR} nanocomposite. CV measurements, performed in the presence of $(Fe(CN)_6)^{3-/4-}$ after each stage of the GCE modification, indicated that (i) pAu could act as tiny conduction centers assisting the electron transfer at the electrode surface and (ii) that GOx/ConA/pAu/Pt–Au/ZnO_{NR}/GCE exhibited an excellent electrocatalytic activity toward glucose. Amperometric measurements in PBS allowed estimating the promising sensor performances.

Guascito *et al.* prepared a composite nanomaterial electrodepositing copper nanoparticles (Cu_{NP}) on an electrosynthesized film of poly-3-methylthiophene (P3MT) [99]. Cu_{NP} were electrodeposited by pulsed potential SWV on both Pt and screen-printed electrodes. The composite film was characterized by SEM and XPS. SEM images proved that pulse amplitude influenced the amount of the deposited particles, but not the Cu_{NP} size. XP spectra relevant to C 1s, Cu 2p, S 2p, Cl 2p, N 1s, O 1s and Na 1s regions were acquired and carefully analyzed both after electropolymerization of 3MT and after electrodepositing Cu_{NP} on the P3MT. C 1s and S 2p signals revealed significantly different compositions of the as-grown P3MT film and of the Cu_{NP}/P3MT composite. The analysis of the complex Cu 2p region required the evaluation of the Auger parameters, which were estimated in the 1846.8–1847.1 eV and 1848.3–1848.8 eV ranges on considering the component of Cu $2p_{3/2}$ at lower and higher BE, respectively. These results allowed excluding the formation of Cu(0) and confirmed the presence of Cu(I) and Cu(II) in each sample. CV and FIA findings showed that the composite film could be applied to the glucose electrochemical detection in flow systems. The response of the sensor to ascorbic acid, uric acid, sorbitol, fructose and dopamine evidenced that it could be effectively used as an electrochemical detector coupled to a chromatographic systems for the simultaneous detection of biomolecules.

Narayanan *et al.* synthesized a nickel nanoparticles (Ni_{NP}) modified electrode in the ionic liquid medium 1-ethyl-3-methylimidazolium ethyl sulfate (EMIMES) for application in biomolecules determinations [100]. Ni_{NP} were electrochemically deposited on a polycysteine film (PCF) previously electropolymerized on a paraffin wax impregnated graphite electrode (PIGE). The Ni_{NP}/PCF/PIGE was characterized by FTIR, Raman, XPS, FESEM, EDS, EIS and CV techniques. The Ni-S bonds evidenced by Raman spectroscopy were further confirmed by XPS survey and detail scans. In particular, the Ni $2p_{3/2}/2p_{1/2}$ doublet (855.6 eV/873.3 eV) and the S $2p_{3/2}$ peak (162.5 eV) were in agreement with the

values reported for NiS. The CV behavior of vitamin B6, L-tyrosine, L-tryptophan, vanillin, glucose and H_2O_2 was studied at the bare PIGE, at the PCF/PIGE and at the Ni_{NP}/PCF/PIGE. This last electrode allowed the best electrocatalytic performances. Good chronoamperometric responses obtained at the Ni_{NP}/PCF/PIGE suggested it could be exploited in flow-systems application.

Khudaish *et al.* prepared a solid-state sensor based on a poly(4-aminodiphenylamine) (Padpa) film deposited at a GCE doped with tris(2,2'-bipyridyl)Ru(II) complex (Padpa/Ru/GCE) [101]. The surface of the CME was characterized by AFM and XPS. AFM images evidenced broken and fused Padpa–Ru doped fiber structures as opposed to those of a native Padpa film, which appeared relatively more uniform. The survey XP spectrum of Padpa showed the presence of carbon, oxygen, nitrogen and ruthenium. The C 1s detail spectrum of the undoped Padpa sample was fitted by three peaks assigned to C–C (283.93 eV), C–N (285.08 eV) and C=C (287.32 eV) bonds. After doping, the Ru $3d_{5/2}/3d_{3/2}$ doublet (280.3 eV/283.2 eV) partially overlapped the C 1s region. The N 1s spectrum of Padpa was also fitted by three peaks assigned to –N= (398.9 eV), $–NH_2$ (400 eV) and NH_3^+ (402.3 eV) nitrogens. The presence of –N= groups confirmed that oxidation and deprotonation processes take place in the polymerization of the Padpa. The electrochemical performances of the CME were tested by CV and DPV. After doping with the Ru(II) complex, CV profiles evidenced reversible redox peaks assigned to the $[Ru(bpy)_3]^{3+/2+}$ couple. The CME was applied to the DPV simultaneous determination of Zn^{2+}, Cd^{2+}, Pb^{2+} and Cu^{2+} ions in sea and ground water samples.

Pan *et al.* synthesized rod-like precursors of Co_3O_4 and Ag/Co_3O_4 composites with different Ag contents via a co-precipitation method [102]. The composites were characterized by TGA/DTA, XRD, TEM, FESEM and XPS. TGA and DTA allowed determining the optimum calcination temperature of the $AgNO_3$ and $Co(NO_3)_2 \cdot 6H_2O$ precursors to obtain the final composites. XPS allowed estimating the surface chemistry of the Ag/Co_3O_4 sample, containing 3% Ag. The Co $2p_{3/2}/2p_{1/2}$ doublet (779.6 eV/795.5 eV; SoS 15.9 eV) were consistent with Co_3O_4 reference data. The Ag $3d_{5/2}/3d_{3/2}$ (367.95 eV/373.9 eV) doublet confirmed the presence of Ag. The experimental Ag/Co molar ratio was very close to the theoretical value, further confirming the composition of the Ag/Co_3O_4 composite with 3% Ag. XRD patterns of Co_3O_4 and Ag/Co_3O_4 were also in good agreement with cubic spinel Co_3O_4 phase. The Co_3O_4/GCE and Ag/Co_3O_4/GCE were tested as sensors for p-nitrophenol reduction in basic solution. At the two CME, the peak current was significantly higher than at a bare GCE. However, at the Ag/Co_3O_4/GCE the peak current increase was also accompanied by a markedly peak potential decrease. The Ag/Co_3O_4 composite with 4% Ag showed the highest electrocatalytic activity.

Guascito *et al.* developed a TeO_2 nanowires modified platinum electrode (TeO_{2NW}/Pt) by drop casting TeO_{2NW}, synthesized by thermal evaporation of Te(0) in oxygen atmosphere, on the substrate surface [103]. The morphological and spectroscopic characterization of TeO_{2NW}, as synthesized on Pt foil, was performed by SEM, XRD and XPS. SEM images showed straight and smooth TeO_{2NW}. Both TeO_{2NW} and a commercial TeO_2 powder standard were analyzed by XPS. Detail scans of the Te $3d_{5/2}$ region of TeO_{2NW} and TeO_2 powder were fitted by peaks assigned to Te(IV) oxide (576.7 ± 0.1 eV) and to Te mixed surface oxides (579.7 ± 0.1 and 579.4 ± 0.1 eV, respectively). Te(0) and Pt(0) were absent. After cycling the TeO_{2NW}/Pt in neutral PBS, XPS evidenced the presence of Te(0) and Te(IV). The electrochemical characterization of the CME was performed by CV and CA in neutral PBS to investigate the sensing properties of this material against H_2O_2. The results proved the catalytic activity

toward hydrogen peroxide reduction and indicated that the TeO_{2NW}/Pt electrode was suitable for sensing applications.

Canevari *et al.* described the preparation of a hybrid material composed of disordered mesoporous silica modified with multiwalled carbon nanotubes [104]. The material was characterized by N_2 adsorption–desorption isotherms, XRD, FESEM, HRTEM, Raman and XPS techniques. HRTEM images showed that MWCNT were embedded within the mesoporous silica matrix. XPS analysis involved exploring the C 1s, O 1s and Si 2p regions. The C 1s region was fitted by peaks assigned to graphitic carbons (284.7 eV), carbon present in alcohol, ether or C=N groups (286.0–286.3 eV), carboxyl or ester groups (288.8–289.1 eV), carbonate groups (290.5–291.2 eV) and satellite peaks due to π–π* transitions in aromatic rings (291.6 eV). The O 1s peak (532.8 eV) was assigned to carbonyl oxygen atoms in esters, anhydrides and oxygen atoms in hydroxyl groups. The Si 2p region originated a signal at 103.5 eV. CMEs were prepared by drop casting a mixture of SiO_2/MWCNT (before and after an acid functionalization) and Nafion® onto GCEs. CV measurements performed in neutral PBS in the presence of the $(Fe(CN)_6)^{3-/4-}$ couple allowed comparing the electrochemical performances of bare GCE and SiO_2/MWCNT/GCE before and after the acid treatment. The CME was applied to individual and simultaneous determinations of dopamine, uric acid and acetaminophen in human urine samples.

In a subsequent study, Canevari *et al.* described synthesis, characterization and applications of a mesoporous silica/multiwalled carbon nanotube (SiO_2/MWCNT) hybrid material, subsequently decorated with silver nanoparticles (Ag_{NP}) [105]. The Ag_{NP}/SiO_2/MWCNT composite was characterized by SEM, EDS, HRTEM and XPS. SEM images and EDS elemental mapping of Ag, C and Si showed a homogeneous distribution of Ag_{NP} in the hybrid material. Detail XP spectra of the composite concerned the Ag 3d, Si 2p, O 1s and C 1s regions. The Ag 3d region was fitted by two Ag $3d_{5/2}/3d_{3/2}$ doublets assigned to Ag(0) (374.4 eV/368.3 eV) and Ag-O species (379.7 eV/373.6 eV), likely due to the formation of Si–O–Ag bonds. These findings were supported by the results of the fitting of O 1s and Si 2p regions. The fitting of the C 1s region also supported the presence of functional groups suitable for anchoring of the Ag_{NP} to the hybrid material. A thin film of Ag_{NP}/SiO_2/MWCNT was deposited on GCEs. The electrochemical performances of the Ag_{NP}/SiO_2/MWCNT/GCE were explored by CV and SWV. In neutral PBS, the sensor showed an excellent electrocatalytic response for the determination of hydroquinone and catechol. Because of the absence of interference from resorcinol, 2,6-dichloroindophenol, phenol, 4-nitrophenol, or nitrite ions, the CME could be applied as a sensor for phenolic compounds in environmental samples.

Guo *et al.* described the electrodeposition of a composite consisting of NiO_{NP} and Pt_{NP} onto electrochemically reduced graphite oxide [106]. The NiO_{NP}/Pt_{NP}/ERGO film was characterized by SEM/EDS, AFM, Raman and XPS techniques. AFM images allowed characterizing the various steps of the preparation of the composite. Detail XP spectra were acquired in the C 1s region of GO and in the C 1s, Pt 4f and Ni 2p regions of the composite. After the electrochemical reduction of GO to ERGO, the C 1s peak assigned to C–C atoms (284.6 eV) increased significantly while those related to the oxidized carbons (C–O, C=O and O=C–O) almost disappeared, thus indicating that oxygen-containing functionalities were nearly completely absent in ERGO. The Pt $4f_{7/2}/4f_{5/2}$ doublet of the NiO_{NP}/Pt_{NP}/ERGO (70.9 eV/74.2 eV) was assigned to Pt(0) while the Ni $2p_{3/2}/2p_{1/2}$ doublet (854.8 eV/872.5 eV; SoS 17.7 eV) was consistent with NiO only. A GCE was electrochemically modified by the NiO_{NP}/Pt_{NP}/ERGO composite. The electrochemical performances of bare GCE,

ERGO/GCE, Pt_{NP}/ERGO/GCE and NiO_{NP}/Pt_{NP}/ERGO/GCE towards glucose oxidation in alkaline medium were compared in NaOH solutions. The results proved that the combination of ERGO, Pt_{NP} and NiO_{NP} led to the highest catalytic efficiency and that the small quantity of Pt_{NP} significantly enhanced the catalytic effect of NiO_{NP}. The proposed CME was applied to glucose detection in real human serum samples.

John *et al.* described the potentiodynamic formation of a gold nanoparticles film on glassy carbon and indium tin oxide (ITO) electrodes by using aminophenyl (APh) diazonium cations grafted gold nanoparticles (APh-Au_{NP}) [107]. The APh-Au_{NP} modified electrodes were characterized by CV, AFM, EIS and XPS. EIS findings proved that the electron transfer reaction of the $(Fe(CN)_6)^{3-/4-}$ couple at the CME was faster than at bare GCE. AFM images showed mono dispersed spherical Au_{NP} attached on the surface of the ITO without undergoing aggregation. The XP survey scan evidenced the presence of C, N and Au on the electrode surface. The Au $4f_{7/2}/4f_{5/2}$ doublet (83.8 eV/87.5 eV; SoS 3.7 eV) proved the presence of Au(0). The N 1s region was fitted by peaks assigned to –NH (396.7 eV), =NH (399.2 eV), $–N^+H$ (400.2 eV) and azo bridges –N=N– (403.3 eV) groups on the APh-Au_{NP} modified ITO substrate. The C 1s region was fitted by three peaks, the one at 286 eV indicating the presence of C–N–bond on the APh-Au_{NP} film modified ITO substrate. CV and DPV measurements allowed verifying that the APh-Au_{NP}/GCE could be applied to the detection of ranitidine hydrochloride (an histamine H_2 receptor antagonist) in the presence of an excess of paracetamol (N-acetyl p-aminophenol). The CME was applied to the detection of the concentration of ranitidine in commercial drugs.

Freire *et al.* prepared hybrid multilayer films composed by osmium metallopolymer $[Os(bpy)_2(PVP)_{10}Cl]Cl$ (Os-poly) and europium phosphomolybdate, $K_{11}[Eu(III)(PMo_{11}O_{39})_2]$ ($Eu(PMo_{11})_2$), by an electrostatic layer-by-layer self-assembly method [108]. Film growth, composition and thickness were monitored by UV-Vis spectroscopy, XPS and SEM. The $\{Os\text{-}poly/Eu(PMo_{11})_2\}_n$ multilayer films (OMF_n) were deposited on quartz slides for UV-Vis and photoluminescence measurements, on glass slides for XPS and on glassy carbon and on ITO/Polyethylene glycol (ITO/PET) electrodes for CV studies. SEM images of OMF_{20} showed a non-uniform distribution of polymeric molecules along with the polyoxometalate (POM) clusters, and allowed measuring film thicknesses. The exhaustive XPS characterization of the composites involved reliable fittings of the C 1s, Os 4f, O 1s, P 2s, Mo 3d, 4f and Eu 3d. Peak positions (BEs) were reported together with the relevant FWHM. In particular, the fitting of the Os $4f_{7/2}/4f_{5/2}$ evidenced the presence of Os^{2+} (50.4 eV/53.2 eV) and Os^{3+} (52.0 eV/54.7 eV). The fitting of the Mo $3d_{5/2}/3d_{3/2}$ region evidenced the presence of Mo^{6+} (253.8 eV/232.6 eV) and Mo^{5+} (234.2 eV/231.1 eV). The presence of 6.1% Mo^{5+} evidenced some photoreduction of POMs under X-ray exposure. XPS findings were completed by surface atomic percentages of the multilayer film. CV measurements obtained at hybrid films adsorbed onto a GCE revealed three Mo-based reduction processes and one Os reduction process in the explored potential range. Cyclic voltammograms of the $(Fe(CN)_6)^{3-/4-}$ and $(Ru(NH))_6^{3+/2+}$ electroactive probes on OMF_n modified electrodes revealed a redox mediation between film and probes and a Mo-based electrocatalytic activity towards reduction of nitrite and iodate.

Guo *et al.* synthesized a series of highly dispersed bimetallic Pt:Pd alloy nanoparticles anchored on RGO with the assistance of the 3-ethyl-1-vinylimidazolium tetrafluoroborate IL [109]. The composite was prepared by ultrasonication of different $H_2PtCl_6/PdCl_2$ mixtures in an IL-GO/ethylene glycol suspension. The composite was characterized by SEM, EDS, TEM, XPS, Raman and XRD techniques.

The overall results demonstrated that Pt:Pd alloy nanoparticles were uniformly dispersed on RGO. In particular, after the reduction, XP spectra of the Pt(50%)Pd(50%)–IL–RGO composite evidenced a clear diminution of the C 1s peak assigned to C–O bonds (286.6 eV) and an increase of the peak assigned to C–C and C=C bonds (284.6 eV). Together with the results of the analysis of the Pt 4f and Pd 3d doublets evidenced in the Pt(50%)Pd(50%)–IL–RGO composite, XPS proved the successful synthesis of the composite. Glucose sensors where prepared by drop casting a composite/Nafion® ink on the surface of GCEs. The electrochemical performances of the Pt(50%)Pd(50%)–IL–RGO/Nafion®/GCE were explored by CV in sulfuric acid solutions. The comparison of the results of amperometric measurements performed in the presence of different glucose concentrations evidenced the superior performances of the proposed CME with respect to some typical enzyme-based glucose sensors, thus making the proposed composite very promising for applications in direct detection of glucose in real human samples.

Scavetta *et al.* prepared a CME by coating ITO electrodes with a ferrocene-functionalized poly(3,4-ethylenedioxythiophene):poly(styrene-4-sulfonate) (PEDOT:PSS) film [110]. The two-step procedure implied the electrodeposition of azidomethyl functionalized 3,4-ethylenedioxythiophene (PEDOT-N_3) followed by copper-catalyzed azide–alkyne cycloaddition of ethynylferrocene. The resulting PEDOT-Fc:PSS conducting polymer was characterized CV, AFM and XPS. Survey XPS scans of PEDOT-N_3:PSS evidenced the presence of the C 1s, O 1s, S 2p and N 1s regions. Authors reported detailed results of the curve fitting (BEs and FWHMs). In particular, the S 2p region of the PEDOT-N_3:PSS coated ITO was fitted by peaks assigned to neutral sulfur of PEDOT (163.7–164.9 eV), cationic S^+ (165.3 eV) associated with the PEDOT backbone and the highly oxidized SO_3^- (167.8–169.0 eV). In the case of the PEDOT-Fc:PSS polymer, the survey scan evidenced the additional Fe 2p region. Together with the results relevant to the N 1s region, XPS proved the partial transformation of the azide group into the 1,2,3-triazole unit bound to the terminal ferrocene head, and the presence of Fe(II) and Fe(III) species. The electrocatalytic behavior of the coating was characterized by the stable and highly reversible response of ferrocene. The linear scan voltammetry in $LiClO_4$ solutions containing different amounts of dopamine proved that ferrocene could mediate the electroxidation of the analyte.

Yang *et al.* developed by a templating approach a hollow CuO polyhedron-modified sensor for the nonenzymatic glucose detection [111]. Morphology and structure of the composite were characterized by FESEM, TEM, XRD, Raman and XPS techniques. XRD results evidenced the standard monoclinic structure of the hollow CuO polyhedron particles. Their hollow interior and structure were also verified by TEM. The purity and composition of the composite were further investigated by XPS. The Cu $2p_{3/2}/2p_{1/2}$ doublet (933.5 eV/953.4 eV) was assigned to CuO. No spectral contribution of Cu_2O was evidenced. The O 1s region was fitted by two peaks assigned to CuO (529.3 eV) and to oxygen adsorbed on the surface of CuO (531.3 eV). The enzyme-free amperometric sensor was prepared by casting a Nafion®-impregnated CuO polyhedron suspension onto a GCE. CV and CA experiments allowed exploring the electrocatalytic activity of the CuO-Nafion®/GCE towards the oxidation of glucose in NaOH solutions. Interfering species such as sodium chloride, ascorbic acid and uric acid did not affect the response of the sensor, which could then find applications as a nonenzymatic glucose sensor.

Pan, Kang *et al.* developed a CME by electropolymerizing alizarin red S (ARS) onto a glassy carbon electrode dipped in the room-temperature ionic liquid 1-butyl-3-methylimidazolium tetrafluoroborate ($BMIMBF_4$) [112]. The polymeric PARS/$BMIMBF_4$ film was characterized by SEM, EDX, XPS, FTIR and electrochemical techniques. SEM images showed that the electropolymerization of ARS in $BMIMBF_4$ led to a smoother and more compact morphology of the coating with respect to that obtained in aqueous solution. EDX results showed that C, B, O, N, F, Si and S were the major elements of the PARS film synthesized in $BMIMBF_4$. In agreement with EDX results, XPS findings relevant to the PARS film confirmed the presence of C, N and S on the composite surface. The comparison of the CV profiles recorded at bare GCEs, PARS/GCEs and PARS/$BMIMBF_4$/GCEs allowed proving that $BMIMBF_4$, owing to its good conductivity, was critical in accelerating electron transfers. The profitable combination of the electrochemical activity of PARS and conductivity of $BMIMBF_4$ allowed the DPV determination of catechol by oxidation to O-quinone in neutral PBS as well as in real water samples.

4. Conclusions

The above papers offer a realistic and diversified panorama about the role played by XPS in the field of electrochemical sensor preparation and characterization. However, some comments are necessary about the interpretation of XPS results. It is evident that some papers report different BE values for the same photoemitting level of the same atomic species in the same chemical state. Examples are the BE values assigned to the Au 4f level of Au(0), or the C 1s BE values assigned to hydrocarbon contamination. These discrepancies could be avoided by a careful selection of literature information. Moreover, in the case of curve fittings of metal-like samples or metal-doped materials, asymmetric peak lineshapes should replace the symmetric ones [113]. This is also the case of the C 1s peak lineshape of graphitic carbons in conductive graphite, carbon nanotubes, and vitreous carbon [24,114,115]. As evidenced in Figure 3, using a symmetrical peak 1 in place of a more correct asymmetrical peak should significantly affect the height of peak 3 (a detailed discussion about how fitting asymmetric lineshapes is reported in Appendix 3 of [16]).

Incorrect fittings could lead to somewhat unreliable conclusions. At last, FWHM and SoS values used in curve fittings should always be reported (see [69] for a good example) but this is rarely done. Canevari *et al.* [104] and Fernandes *et al.* [108] are appreciable examples of correctly reporting the results of XPS curve fittings.

The reviewed papers are of sanitary, pharmacological, alimentary and environmental concern. Tables 2 and 3 itemize the XPS-characterized sensors, which are suitable for food and environmental analysis, respectively.

In conclusion, notwithstanding the above-mentioned comments, XPS always offers an unrivalled help in controlling the composition of the ultimate surface layers of the sensor as well as in following the evolution of surface functionalities during its preparation. Hopefully, the above described results could induce more researchers to consider XPS as a key technique to achieve important surface information for characterizing and optimizing the sensors.

Table 2. Examples of applications of the reviewed chemically modified electrodes (CMEs) in food analysis.

Application	References
Carbohydrates sensor in real samples (milk, fruit juice)	[28]
Carbohydrates sensor	[29]
Biosensor for alcohol content in various beverages	[46]
Sensor for bromate (fermented beverages, fish pastes, drinking water)	[57]
Sensor for aflatoxin	[64]
Sensor for hydrogen peroxide and Cu^{2+}	[65]
Sensor for xanthine, hypoxanthine in commercial fresh chicken and flesh	[73]
Tartrazine (food colorant) sensor	[82]
Cysteine sensor	[86]
Nitrite sensor	[90]
Sensor for vitamin B_6, L-tyrosine, L-tryptophan, vanillin, glucose, H_2O_2	[100]

Table 3. Examples of environmental applications of the reviewed CMEs.

Application	References
Removal of m-nitroaniline from aqueous solutions	[37]
Bromate sensor and elimination in water solutions.	[61]
Degradation of organic dyes eluted from textile industries	[62]
Sensor for hydrogen peroxide	[65]
Hydrazine sensor	[67]
Hg(II) in tap and river water samples	[71]
Sensor for NO from automotive catalytic converters	[89]
Nitrite sensor	[90]
Formaldehyde sensor (in atmosphere and exhausts)	[92]
Cs^+ selective ion-exchange devices for radioactive liquid waste	[94]
Sensor for simultaneous analysis of Zn^{2+}, Cd^{2+}, Pb^{2+}, Cu^{2+} in water samples	[101]
p-nitrophenol sensor	[102]
Sensor for dihydroxybenzenes in untreated river water	[105]
Sensor for catechol in real water samples	[112]

Appendix

3APCP	3-aminophenylcalix[4]pyrrole
3MT	3-methylthiophene
AA	Ascorbic Acid
AFM	Atomic Force Microscopy
ALD	Atomic Layer Deposition
AMT	5-amino-2-mercapto-1,3,4-thiadiazole
Aox	Alcohol oxidase
AP	Allopurinol
APh	Aminophenil
ARS	Alizarin red S

ATP	Aminothiophenol
ATR-FTIR	Attenuated Total Reflectance-FTIR
BA	Benzoic acid
BE	Binding energy
BIPN	2-(4-nitrophenyl)-4,7-di(thiophene-2-yl)-1H-benzo[d]imidazole
$BMIMBF_4$	1-butyl-3-methylimidazolium tetrafluoroborate
BMIM-Cl	1-butyl-3-methylimidazolium chloride
BSA	Bovine Serum Albumin
Bupy-Cl	1-butylpyridinium chloride
CA	Chronoamperometry
CDSI	Cyclic Disulfide
CME	Chemically Modified Electrode
CNT	Carbon Nanotube
CV	Cyclic Voltammetry
DA	Dopamine
DMF	Dymethylformamide
DMSO	Dimethylsulfoxide
DPV	Differential Pulse Voltammetry
DRS	Diffuse Reflectance Spectroscopy
DTA	Differential Thermal Analysis
EDAX	Energy Dispersive X-ray Analysis
EDC	3-(3-dimethylaminopropyl)-1-ethylcarbodiimide hydrochloride
EDOT-N_3	Azidomethyl functionalized 3,4-ethylenedioxythiophene
EDS	Energy Dispersive X-ray Spectroscopy (also mentioned as EDX)
EELS	Electron Energy Loss Spectroscopy
EIS	Electrochemical Impedance Spectroscopy
EMIMES	1-ethyl-3-methylimidazolium ethyl sulfate
EQCM	Electrochemical Quartz Crystal Microbalamce
ERGO	Electrochemically Reduced Graphene Oxide
ES	Electrode Surface
ESCA	Electron Spectroscopy for Chemical Analysis
ESI-MS	Electrospray Ionisation Mass Spectrometry
FESEM	Field Emission SEM
FIA	Flow Injection Analysis
FTIR	Fourier Transform IR
FTO	Fluorine-doped Tin Oxide
FWHM	Full Width at Half Maximum
GA	Glutaraldehyde
GCE	Glassy Carbon Electrode
GO	Graphite Oxide/Graphene Oxide

GOD	Glucose Oxidase
GR	Graphene (also indicated as rGO – reduced GO)
HDA	1,6-hexanediamine
HNPs	Heterodimer Nanoparticles
HOMO	Highest Occupied Molecular Orbital
HOPG	Highly Oriented Pyrolitic Graphite
HQ	Hydroquinone
HQSA	8-hydroxyquinoline-5-sulphonic acid
HRTEM	High Resolution TEM
KE	Kinetic Energy
IL	Ionic Liquid
IRRAS	Infrared Reflection-Absorption Spectroscopy
ITO	Indium Tin Oxide
LMM	L-inner level-M-inner level-M-inner level Auger transition
LSV	Linear Scan Voltammetry
LUMO	Lowest Unoccupied Molecular Orbital
MB	Methylene Blue
MHCF	Metal hexacyanoferrate
MOR	Methanol oxidation reaction
MPA	3-mercaptopropionic acid
μT	Micro Tubes
MWCNT	Multi-Walled CNT
NA	Nafion®
Nap	Naproxene
NBM	3-(nitrobenzyl)mercaptan
NC	Nano Cubes
NCL	Nano Clusters
NF	Nano Fibers
NHS	N-hydroxysuccinimide
NL	Nano Leaves
NMR	Nuclear Magnetic Resonance
NP	Nano Particles
NPD	4-nitrophenyl diazonium
NR	Nano Rod
NRed	Neutral Red
NS	Nano Seeds, Nano Sheets
NSSFs	self-standing nanostructured silver fibres
NT	Nano Tubes
OMF	Osmium Multilayer Film
p(BCP)	Poly Bromocresol Purple

PAD	Pulsed Amperometric Detection
Padpa	poly(4-aminodiphenylamine)
PAMAM	Poly(amidoamine)
PANI	Poly-aniline
PAR	Peaks Area Ratio
PB	Prussian Blue
PBS	Phosphate Buffer Solution
PC	Photocatalytic
PCF	Polycysteine
PDDA	Poly(diallyldimethyl)ammonium chloride
PEC	Photoelectrocatalytic
PEDOT	Poly(3,4-ethylenedioxythiophene)
PET	Polyethylene glycol
PIGE	Paraffin wax Impregnated Graphite Electrode
PImox	Overoxidized Polyimidazole
PMEL	Poly(melamine)
PM-IRRAS	Polarization Modulation Infrared Reflection-Absorption Spectroscopy
POM	Polyoxometallates
PPUA	poly(11-N-pyrrolylundecanoic) acid
PPY	Polypyrrole
PSS	Poly(styrene-4-sulfonate)
PUP	Poly(N-undecylpyrrole)
PV4P	Poly(4-vinylpyridine)
PVA	Polyvinylalcohol
Py	1-aminopyrene
PW	Phosphotungstic acid
RAIRS	Reflection-Absorption Infrared Spectroscopy
RDE	Rotating Disk Electrode
RTIL	Room Temperature Ionic Liquid
rGO	reduced Graphene Oxide
R_{rms}	Root mean squared Roughness
SAED	Selected-Area Electron Diffraction
SAM	Self-assembled monolayer
SECM	Scanning Electrochemical Microscopy
SEM	Scanning Electron Microscopy
SHG	Second Harmonic Generation
SIMS	Secondary Ions Mass Spectrometry
SoS	Spin Orbit Splitting
SPCE	Screen Printed Carbon Electrode
SPE	Screen Printed Electrode

SWV	Square Wave Voltammetry
$TBAPF_6$	Tetrabutylammonium hexafluorophosphate
TBATFB	Tetrabutylammonium tetrafluoroborate
TEM	Trasmission Electron Microscopy
TGA	Thermogravimetric Analysis
ThL	*Trametes hirsuta* laccase
TMB	3, 3′, 5, 5′-tetramethylbenzidine
TNT	Titanate Nanotubes
UA	Uric Acid
UOx	Uricase
UV-Vis	Ultraviolet-Visible Spectroscopy
XP	X-ray Photoelectron
XPS	X-ray Photoelectron Spectroscopy
XRD	X-ray Diffraction
XRF	X-ray Fluorescence

Acknowledgments

Financial support by COFIN 2010–2011 (Programmi di Ricerca Scientifica di Rilevante Interesse Nazionale, MIUR, 2010AXENJ8_002) is acknowledged.

Conflicts of Interest

The authors declare no conflict of interest.

References

1. Durst, R.A.; Bäumner, A.J.; Murray, R.W.; Buck, R.P.; Andrieux, C.P. Chemically modified electrodes: Recommended terminology and definitions. *Pure Appl. Chem.* **1997**, *69*, 1317–1323.
2. Kutner, W.; Wang, J.; L'Her, M.; Buck, R.P. Analytical aspects of chemically modified electrodes: Classification, critical evaluation and recommendations. *Pure Appl. Chem.* **1998**, *70*, 1301–1318.
3. Belding, S.R.; Campbell, F.W.; Dickinson, E.J.F.; Compton, R.G. Nanoparticle-modified electrodes. *Phys. Chem. Chem. Phys.* **2010**, *12*, 11208–11221.
4. Oyama, M. Recent nanoarchitectures in metal nanoparticle-modified electrodes for electroanalysis. *Anal. Sci.* **2010**, *26*, 1–12.
5. Radi, A.-E. Recent Updates of Chemically Modified Electrodes in Pharmaceutical Analysis. *Comb. Chem. High Throughput Screen.* **2010**, *13*, 728–752.
6. Merkoçi, A. Nanoparticles-based strategies for DNA, protein and cell sensors. *Biosens. Bioelectron.* **2010**, *26*, 1164–1177.
7. Toghill, K.E.; Compton, R.G. Metal Nanoparticle Modified Boron Doped Diamond Electrodes for Use in Electroanalysis. *Electroanalysis* **2010**, *22*, 1947–1956.
8. Arduini, F.; Calvo, J.Q.; Palleschi, G.; Moscone, D.; Amine, A. Bismuth-modified electrodes for lead detection. *TrAC* **2010**, *29*, 1295–1304.

9. Rad, A.S.; Mirabi, A.; Binaian, E.; Tayebi, H. A Review on Glucose and Hydrogen Peroxide Biosensor Based on Modified Electrode Included Silver Nanoparticles. *Int. J. Electrochem. Sci.* **2011**, *8*, 3671–3683.
10. Brownson, D.A.C.; Foster, C.W.; Banks, C.E. The electrochemical performance of graphene modified electrodes: An analytical perspective. *Analyst* **2012**, *137*, 1815–1823.
11. Ciucu, A.A. Chemically Modified Electrodes in Biosensing. *J. Biosens. Bioelectron.* **2014**, *5*, 1–10.
12. Desimoni, E.; Brunetti, B. Glassy Carbon Electrodes Film-Modified with Acidic Functionalities. A Review. *Electroanalysis* **2012**, *24*, 1481–1500.
13. Walcarius, A. Electrocatalysis, sensors and biosensors in analytical chemistry based on ordered mesoporous and macroporous carbon-modified electrodes. *TrAC* **2012**, *38*, 79–97.
14. Doyle, R.L.; Godwin, I.J.; Brandon, M.P.; Lyons, M.E.G. Redox and electrochemical water splitting catalytic properties of hydrated metal oxide modified electrodes. *Phys. Chem. Chem. Phys.* **2013**, *15*, 13737–13783.
15. Martin, A.; Escarpa, A. Graphene: The cutting edge interaction between chemistry and electrochemistry. *TrAC* **2014**, *56*, 13–26.
16. Briggs, D.; Seah, M.P. *Practical Surface Analysis*, 2nd ed.; J. Wiley & Sons: Chichester, UK, 1990; Volume 1.
17. Desimoni, E.; Zambonin, P.G. Spectroscopies for surface characterization. In *Surface Characterization of Advanced Polymers*; Sabbatini, L., Zambonin, P.G., Eds.; VCH: Weinheim, Germany, 1993; pp. 1–45.
18. Riviere, J.C.; Myhra, S. *Handbook of Surface and Interface Analysis: Methods for Problem-Solving*, 2nd ed.; CRC Press: Boca Raton, FL, USA, 2009; pp. 1–64.
19. Hüfner, S. Photoelectron Spectroscopy: Principles and Applications, 3rd ed.; Springer: Berlin, Germany, 2003.
20. Hofman, S. Auger- and X-Ray Photoelectron Spectroscopy in Materials Science: A User-Oriented Guide; Springer, Berlin, Germany, 2012.
21. Van der Heide, P. X-Ray Photoelectron Spectroscopy: An Introduction to the Principles and Practices; Wiley: Chichester, UK, 2012.
22. Bagus, P.S.; Ilton, E.S.; Nelin, C.J. The interpretation of XPS spectra: Insights into materials properties. *Surf. Sci. Rep.* **2013**, *68*, 273–304.
23. Brunetti, B.; de Giglio, E.; Cafagna, D.; Desimoni, E. XPS analysis of glassy carbon electrodes chemically modified with 8-hydroxyquinoline-5-sulphonic acid. *Surf. Interface Anal.* **2012**, *44*, 491–496.
24. Desimoni, E.; Salvi, A.M.; Casella, I.G.; Damiano, D. Controlled chemical oxidation of carbon fibres: An XPS-XAES-SEM study. *Surf. Interface Anal.* **1993**, *20*, 909–918.
25. Beamson, G.; Briggs, D. *High Resolution XPS of Organic Polymers*; J. Wiley & Sons: Chichester, UK, 1992.
26. Crist, B.V. Handbook of Monochromatic XPS Spectra, Polymers and Polymers Damagedby X-Rays; J. Wiley & Sons: Chichester, UK, 2000.
27. Desimoni, E.; Malitesta, C.; Zambonin, P.G.; Riviere, J.C. An X-ray photoelectron spectroscopic study of some cromium-oxygen systems. *Surf. Interface Anal.* **1988**, *13*, 173–179.

28. Casella, I.G.; Desimoni, E.; Castaldi, T.R.I. Study of a nickel-catalysed glassy carbon electrode for detection of carbohydrates in liquid chromatography and flow injection analysis. *Anal. Chim. Acta* **1991**, *248*, 117–125.
29. Cataldi, T.R.I.; Casella, I.G.; Desimoni, E.; Rotunno, T. Co-based Glassy Carbon CME for Constant-Potential Amperometric Detection of Carbohydrates in FIA and Liquid Chromatography. *Anal. Chim. Acta* **1992**, *270*, 161–171.
30. Casella, I.G.; Desimoni, E. XPS, SEM and electrochemical characterization of a platinum-based glassy carbon modified electrode. Electrocatalytic oxidation of ethanol in acidic medium. *Electroanalysis* **1996**, *8*, 447–453.
31. Taouil, A.E.; Lallemand, F.; Melot, J.; Husson, J.; Hihn, J.; Lakard, B. Effects of polypyrrole modified electrode functionalization on potentiometric pH responses. *Synth. Met.* **2010**, *160*, 1073–1080.
32. Li, S.; Yang, Y.; Yang, S.; Ye, S.; Fang, H.; Hu, J.; Li, Q. Electrochemical reduction and voltammetric determination of pirarubicin at carboxyl ions implantation-modified indium tin oxide electrode. *Chin. J. Anal. Chem.* **2011**, *39*, 990–993.
33. Xue, Y.; Zhao, H.; Wu, Z.; Li, X.; He, Y.; Yuan, Z. The comparison of different gold nanoparticles/graphene nanosheets hybrid nanocomposites in electrochemical performance and the construction of a sensitive uric acid electrochemical sensor with novel hybrid nanocomposites. *Biosens. Bioelectron.* **2011**, *29*, 102–108.
34. Sundaram, S.; Annamalai, S.K. Selective immobilization of hydroquinone on carbon nanotube modified electrode via phenol electro-oxidation method and its hydrazine electro-catalysis and *Escherichia coli* antibacterial activity. *Electrochim. Acta* **2012**, *62*, 207–217.
35. Wei, L.; Lei, Y.; Fu, H.; Yao, J. Fullerene hollow microspheres prepared by bubble-templates as sensitive and selective electrocatalytic sensor for biomolecules. *ACS Appl. Mater. Interfaces* **2012**, *4*, 1594–1600.
36. Valentini, F.; Roscioli, D.; Carbone, M.; Conte, V.; Floris, B.; Palleschi, G.; Flammini, R.; Bauer, E.M.; Nasillo, G.; Caponetti, E. Oxidized graphene in ionic liquids for assembling chemically modified electrodes: A structural and electrochemical characterization study. *Anal. Chem.* **2012**, *84*, 5823–5831.
37. Ding, L.; Li, Q.; Zhou, D.; Cui, H.; Tang, R.; Zhai, J. Copolymerization of aniline with m-nitroaniline and removal of m-nitroaniline from aqueous solutions using a polyaniline-modified electrode: A comparative study. *Electrochim. Acta* **2012**, *77*, 302–308.
38. Demirci, S.; Emre, F.B.; Ekiz, F.; Oğuzkaya, F.; Timur, S.; Tanyeli, C.; Toppare, L. Functionalization of poly-SNS-anchored carboxylic acid with Lys and PAMAM: Surface modifications for biomolecule immobilization/stabilization and bio-sensing applications. *Analyst* **2012**, *137*, 4254–4261.
39. Yang, J.; Myoung, N.; Hong, H. Facile and controllable synthesis of Prussian blue on chitosan-functionalized graphene nanosheets for the electrochemical detection of hydrogen peroxide. *Electrochim. Acta* **2012**, *81*, 37–43.
40. Baskar, S.; Liao, C.; Chang, J.; Zen, J. Electrochemical synthesis of electroactive poly(melamine) with mechanistic explanation and its applicability to functionalize carbon surface to prepare nanotube–nanoparticles hybrid. *Electrochim. Acta* **2013**, *88*, 1–5.

41. You, J.; Kim, D.; Kim, S.K.; Kim, M.; Han, H.S.; Jeon, S. Novel determination of hydrogen peroxide by electrochemically reduced graphene oxide grafted with aminothiophenol–Pd Nanoparticles. *Sens. Actuators B Chem.* **2013**, *178*, 450–457.
42. Raj, M.A.; John, S.A. Fabrication of electrochemically reduced graphene oxide films on glassy carbon electrode by self-assembly method and their electrocatalytic application. *J. Phys. Chem. C* **2013**, *117*, 4326–4335.
43. Guo, K.; Chen, X.; Freguia, S.; Dolose, B.C. Spontaneous modification of carbon surface with neutral red from its diazonium salts for bioelectrochemical systems. *Biosens. Bioelectron.* **2013**, *47*, 184–189.
44. Ghilane, J.; Hauquier, F.; Lacroix, J. Oxidative and stepwise grafting of dopamine inner-sphere redox couple onto electrode material: Electron transfer activation of dopamine. *Anal. Chem.* **2013**, *85*, 11593–11601.
45. Raj, M.A.; John, S.A. Electrochemical determination of xanthine oxidase inhibitor drug in urate lowering therapy using graphene nanosheets modified electrode. *Electrochim. Acta* **2014**, *117*, 360–366.
46. Soylemez, S.; Kanik, F.E.; Uzun, S.D.; Hacioglu, S.O.; Toppare, L. Development of an efficient immobilization matrix based on a conducting polymer and functionalized multiwall carbon nanotubes: Synthesis and its application to ethanol biosensors. *J. Mater. Chem. B* **2014**, *2*, 511–521.
47. Si, W.; Lei, W.; Han, Z.; Zhang, Y.; Hao, Q.; Xia, M. Electrochemical sensing of acetaminophen based on poly(3,4-ethylenedioxythiophene)/graphene oxide composites. *Sens. Actuators B Chem.* **2014**, *193*, 823–829.
48. Yang, L.; Liu, D.; Huang, J.; You, T. Simultaneous determination of dopamine, ascorbic acid and uric acid at electrochemically reduced graphene oxide modified electrode. *Sens. Actuators B Chem.* **2014**, *193*, 166–172.
49. Zong, X.; Kong, N.; Liu, J.; Yang, W.; Cao, M.; Gooding, J.J. The influence of graphene on the electrical communication through organic layers on graphite and gold electrodes. *Electroanalysis* **2014**, *26*, 84–92.
50. Liu, X.; Zhang, L.; Wei, S.; Chen, S.; Ou, X.; Lu, Q. Overoxidized polyimidazole/graphene oxide copolymer modified electrode for the simultaneous determination of ascorbic acid, dopamine, uric acid, guanine and adenine. *Biosens. Bioelectron.* **2014**, *57*, 232–238.
51. Felix, S.; Kollu, P.; Raghupathy, B.P.C.; Jeong, S.K.; Grace, A.N. Electrocatalytic activity of Cu_2O nanocubes-based electrode for glucose oxidation. *J. Chem. Sci.* **2014**, *126*, 25–32.
52. Le Goff, A.; Moggia, F.; Debou, N.; Jegou, P.; Artero, V.; Fontecave, M.; Jousselme, B.; Palacin, S. Facile and tunable functionalization of carbon nanotube electrodes with ferrocene by covalent coupling and π-stacking interactions and their relevance to glucose bio-sensing. *J. Electroanal. Chem.* **2010**, *641*, 57–63.
53. Sharifi, N.; Tajabadi, F.; Taghavinia, N. Nanostructured silver fibers: Facile synthesis based on natural cellulose and application to graphite composite electrode for oxygen reduction. *Int. J. Hydrogen Energ.* **2010**, *35*, 3258–3262.

54. Che, X.; Yuan, R.; Chai, Y.; Li, J.; Song, Z.; Li, W. Amperometric glucose biosensor based on Prussian blue–multiwall carbon nanotubes composite and hollow PtCo nanochains. *Electrochim. Acta* **2010**, *55*, 5420–5427.
55. Guascito, M.R.; Chirizzi, D.; Picca, R.A.; Mazzotta, E.; Malitesta, C. Ag nanoparticles capped by a nontoxic polymer: Electrochemical and spectroscopic characterization of a novel nanomaterial for glucose detection. *Mater. Sci. Eng. C* **2011**, *31*, 606–611.
56. Guascito, M.R.; Chirizzi, D.; Malitesta, C.; Mazzotta, E.; Siciliano, M.; Siciliano, T.; Tepore, A.; Turco, A. Low-potential sensitive H_2O_2 detection based on composite micro tubular Te adsorbed on platinum electrode. *Biosens. Bioelectron.* **2011**, *26*, 3562–3569.
57. Zhou, D.; Ding, L.; Cui, H.; An, H.; Zhai, J.; Li, Q. Fabrication of high dispersion Pd/MWNTs nanocomposite and its electrocatalytic performance for bromate determination. *Chem. Eng. J.* **2012**, *200–202*, 32–38.
58. Guascito, M.R.; Chirizzi, D.; Malitesta, C.; Siciliano, M.; Siciliano, T.; Tepore, A. Amperometric non-enzymatic bimetallic glucose sensor based on platinum tellurium microtubes modified electrode. *Electrochem. Commun.* **2012**, *22*, 45–48.
59. Devaraj, M.; Deivasigamani, R.K.; Jeyadevan, S. Enhancement of the electrochemical behavior of CuO nanoleaves on MWCNT/GC composite film modified electrode for determination of norfloxacin. *Colloids Surf. B* **2013**, *102*, 554–561.
60. Kim, H.J.; Kwon, S.; Kim, K. Electrochemically active cyclic disulfide-ended organic silane linkage for preparation of multi-biofunctional electrode surfaces. *Electrochem. Commun.* **2012**, *20*, 52–55.
61. Li, Q.; Zhang, Q.; Ding, L.; Zhou, D.; Cui, H.; Wei, Z.; Zhai, J. Synthesis of Silver/multi-walled carbon nanotubes composite and its application for electrocatalytic reduction of bromate. *Chem. Eng. J.* **2013**, *217*, 28–33.
62. Chatchai, P.; Nosaka, A.Y.; Nosaka, Y. Photoelectrocatalytic performance of WO_3/$BiVO_4$ toward the dye degradation. *Electrochim. Acta* **2013**, *94*, 314–319.
63. Tian, H.; Jia, M.; Zhang, M.; Hu, J. Nonenzymatic glucose sensor based on nickel ion implanted-modified indium tin oxide electrode. *Electrochim. Acta* **2013**, *96*, 285–290.
64. Singh, J.; Roychoudhury, A.; Srivastava, M.; Solanki, P.R.; Lee, D.W.; Lee, S.H.; Malhotra, B.D. A highly efficient rare earth metal oxide nanorods based platform for aflatoxin detection. *J. Mater. Chem. B* **2013**, *1*, doi:10.1039/c3tb20690d.
65. Tanwar, S.; Ho, J.A.; Magi, E. Green synthesis and characterization of novel gold nanocomposites for electrochemical sensing applications. *Talanta* **2013**, *117*, 352–358.
66. Fu, Y.; Liang, F.; Tian, H.; Hu, J. Nonenzymatic glucose sensor based on ITO electrode modified with gold nanoparticles by ion implantation. *Electrochim. Acta* **2014**, *120*, 314–318.
67. Koçak, S.; Aslışen, B. Hydrazine oxidation at gold nanoparticles and poly(bromocresol purple) carbon nanotube modified glassy carbon electrode. *Sens. Actuators B Chem.* **2014**, *196*, 610–618.
68. Kumar, D.R.; Manoj, D.; Santhanalakshmi, J. Au–ZnO bullet-like heterodimer nanoparticles: Synthesis and use for enhanced nonenzymatic electrochemical determination of glucose. *RSC Adv.* **2014**, *4*, 8943–8952.

69. Derouich, S.G.; Rinfray, C.; Izzet, G.; Pinson, J.; Gallet, J.; Kanoufi, F.; Proust, A.; Combellas, C. Control of the grafting of hybrid polyoxometalates on metal and carbon surfaces: Toward submonolayers. *Langmuir* **2014**, *30*, 2287–2296.
70. Piotrowski, P.; Pawłowska, J.; Pawłowski, J.; Więckowska, A.; Bilewicz, R.; Kaim, A. Nanostructured films of *in situ* deprotected thioacetyl-functionalized C60-fullerenes on a gold surface. *J. Mater. Chem. A* **2014**, *2*, 2353–2362.
71. Gong, J.; Zhou, T.; Song, D.; Zhang, L.; Hu, X. Stripping voltammetric detection of mercury(II) based on a bimetallic Au-Pt inorganic-organic hybrid nanocomposite modified glassy carbon electrode. *Anal. Chem.* **2010**, *82*, 567–573.
72. Melato, A.I.; Abrantes, L.M.; Botelho do Rego, A.M. $Fe(CN)_6^{3-}$ incorporation on Poly(3,4-ethylenedioxythiophene) films: Preparation and X-ray photoelectron spectroscopy characterization of the modified electrodes. *Thin Solid Films* **2010**, *518*, 1947–1952.
73. Kumar, A.S.; Swetha, P. $Ru(DMSO)_4Cl_2$ nano-aggregated Nafion membrane modified electrode for simultaneous electrochemical detection of hypoxanthine, xanthine and uric acid. *J. Electroanal. Chem.* **2010**, *642*, 135–142.
74. Wang, J.; Xu, M.; Zhao, R.; Chen, G. A highly sensitive H_2O_2 sensor based on zinc oxide nanorod arrays film sensing interface. *Analyst* **2010**, *135*, 1992–1996.
75. Sosna, M.; Chrétien, J.-M.; Kilburn, J.D.; Bartlett, P.N. Monolayer anthracene and anthraquinone modified electrodes as platforms for *Trametes hirsuta* laccase immobilization. *Phys. Chem. Chem. Phys.* **2010**, *12*, 10018–10026.
76. Lin, L.; Huang, X.; Wang, L.; Tang, A. Synthesis, characterization and the electrocatalytic application of prussian blue/titanate nanotubes nanocomposite. *Solid State Sci.* **2010**, *12*, 1764–1769.
77. Xing, L.; Jia, J.; Wang, Y.; Zhang, B.; Dong, S. Pt modified TiO_2 nanotubes electrode: Preparation and electrocatalytic application for methanol oxidation. *Int. J. Hydrogen Energ.* **2010**, *35*, 12169–12173.
78. Lokesh, K.S.; de Wael, K.; Adriaens, A. Self-Assembled Supramolecular Array of polymeric phthalocyanine on gold for the determination of hydrogen peroxide. *Langmuir* **2010**, *26*, 17665–17673.
79. Fontaine, O.; Ghilane, J.; Martin, P.; Lacroix, J.-C.; Randriamahazaka, H. Ionic liquid viscosity effects on the functionalization of electrode material through the electroreduction of diazonium. *Langmuir* **2010**, *26*, 18542–18549.
80. Feliciano-Ramos, I.; Caban-Acevedo, M.; Scibioh, M.A.; Cabrera, C.R. Self-assembled monolayers of L-cysteine on palladium electrodes. *J. Electroanal. Chem.* **2010**, *650*, 98–104.
81. Im, J.; Han, J.; Kim, B.K.; Han, J.H.; Park, T.S.; Hwang, S.; Cho, S.I.; Lee, W.; Kim, Y. Electrochemical detection of estrogen hormone by immobilized estrogen receptor on Au electrode. *Surf. Coat. Technol.* **2010**, *205*, S275–S278.
82. Brunetti, B.; Desimoni, E. A new voltammetric sensor based on a glassy carbon electrode modified with 8-hydroxyquinoline-5-sulfonic acid. *Electroanalysis* **2011**, *23*, 1116–1122.

83. Ganesh, V.; Maheswari, D.L.; Berchmans, S. Electrochemical behaviour of metal hexacyanoferrate converted to metal hydroxide films immobilized on indium tin oxide electrodes—Catalytic ability towards alcohol oxidation in alkaline medium. *Electrochim. Acta* **2011**, *56*, 1197–1207.
84. Pchelintsev, N.A.; Vakurov, A.; Hays, H.H.; Millner, P.A. Thiols deposition onto the surface of glassy carbon electrodes mediated by electrical potential. *Electrochim. Acta* **2011**, *56*, 2696–2702.
85. Liu, L.; Wang, S.; Zhu, Z.; Li, M.; Sun, B. Electrochemistry of a C_{84}-C_2(IV)-Modified Electrode in Aqueous Solutions and Its Interaction with Guanine. *J. Phys. Chem. C* **2011**, *115*, 5966–5973.
86. Hsiao, Y.; Su, W.; Cheng, J.; Cheng, S. Electrochemical determination of cysteine based on conducting polymers/gold nanoparticles hybrid nanocomposites. *Electrochim. Acta* **2011**, *56*, 6887–6895.
87. Kannan, P.; John, S.A. Fabrication of conducting polymer-gold nanoparticles film on electrodes using monolayer protected gold nanoparticles and its electrocatalytic application. *Electrochim. Acta* **2011**, *56*, 7029–7037.
88. Feng, X.; Li, R.; Ma, Y.; Chen, R.; Shi, N.; Fan, Q.; Huang, W. One-Step Electrochemical Synthesis of Graphene/Polyaniline Composite Film and Its Applications. *Adv. Funct. Mater.* **2011**, *21*, 2989–2996.
89. Zhang, R.; Li, L.; Chen, L.; Zhang, G.; Shi, K. N-doped carbon nanotubes synthesized in high yield and decorated with CeO_2 and SnO_2 nanoparticles. *J. Alloys Compd.* **2011**, *509*, 8620–8624.
90. Yuan, J.; Jin, X.; Li, N.; Chen, J.; Miao, J.; Zhang, Q.; Niu, L.; Song, J. Large scale load of phosphotungstic acid on multiwalled carbon nanotubes with a grafted poly(4-vinylpyridine) linker. *Electrochim. Acta* **2011**, *56*, 10069–10076.
91. Taner, B.; Deveci, P.; Üstündağ, Z.; Keskin, S.; Özcan, E.; Solak, A.O. Modification of glassy carbon electrode by the electrochemical oxidation of 3-aminophenylcalix[4]pyrrole in nonaqueous media. *Surf. Interface Anal.* **2012**, *44*, 185–191.
92. Tanwar, S.; Chuang, M.-C.; Prasad, K.S.; Ho, J.-A.A. Template-free synthesis of an electroactive Au-Calix-PPY nanocomposite for electrochemical sensor applications. *Green Chem.* **2012**, *14*, 799–808.
93. Li, X.; Kong, F.; Liu, J.; Liang, T.; Xu, J.; Chen, H. Synthesis of potassium-modified graphene and its application in nitrite-selective sensing. *Adv. Funct. Mater.* **2012**, *22*, 1981–1988.
94. Li, N.; Li, Z.; Yuan, J.; Hu, J.; Miao, J.; Zhang, Q.; Niub, L.; Song, J. Nickel hexacyanoferrate nanoparticles anchored to multiwalled carbon nanotubes with a grafted poly(4-vinylpyridine) linker for electrically switched ion exchange. *Electrochim. Acta* **2012**, *72*, 150–156.
95. Wang, B.; Li, Y.; Qin, X.; Zhan, G.; Ma, M.; Li, C. Electrochemical fabrication of TiO_2 nanoparticles/[BMIM]BF_4 ionic liquid hybrid film electrode and its application in determination of p-acetaminophen. *Mat. Sci. Eng. C* **2012**, *32*, 2280–2285.
96. Sun, Z.; Fu, H.; Deng, L.; Wang, J. Redox-active thionine–graphene oxide hybrid nanosheet: One-pot, rapid synthesis, and application as a sensing platform for uric acid. *Anal. Chim. Acta* **2013**, *761*, 84–91.
97. Bettge, M.; Li, Y.; Sankaran, B.; Rago, N.D.; Spila, T.; Haasch, R.T.; Petrov, I.; Abraham, D.P. Improving high-capacity $Li_{1.2}Ni_{0.15}Mn_{0.55}Co_{0.1}O_2$-based lithium-ion cells by modifying the positive electrode with alumina. *J. Power Sources* **2013**, *233*, 346–357.

98. Zhang, J.; Wang, C.; Chen, S.; Yuan, D.; Zhong, X. Amperometric glucose biosensor based on glucose oxidase–lectin biospecific interaction. *Enzyme Microb. Technol.* **2013**, *52*, 134–140.
99. Malitesta, C.; Guascito, M.R.; Mazzotta, E.; Siciliano, T.; Tepore, A. Copper nanoparticles/ poly-3-methylthiophene composite: Synthesis, characterization and catalytic application to enzyme-less glucose detecting. *Sens. Actuators B Chem.* **2013**, *184*, 70–77.
100. Babu, R.S.; Prabhu, P.; Narayanan, S.S. Green synthesized nickel Nanoparticles modified electrode in ionic liquid medium and its application towards determination of biomolecules. *Talanta* **2013**, *110*, 135–143.
101. Khudaish, E.A.; Al-Hinaai, M.M.; Al-Harthi, S.H. A solid-state sensor based on tris(2,2'-bipyridyl)ruthenium(II)/poly(4-aminodiphenylamine) modified electrode: Characterization and applications. *Sens. Actuators B Chem.* **2013**, *185*, 478–487.
102. Pan, L.; Tang, J.; Wang, F. Synthesis and electrocatalytic performance for p-nitrophenol reduction of rod-like Co_3O_4 and Ag/Co_3O_4 composites. *Mater. Res. Bull.* **2013**, *48*, 2648–2653.
103. Guascito, M.R.; Chirizzi, D.; Malitesta, C.; Siciliano, T.; Tepore, A. Te oxide nanowires as advanced materials for amperometric nonenzymatic hydrogen peroxide sensing. *Talanta* **2013**, *115*, 863–869.
104. Canevari, T.C.; Raymundo-Pereira, P.A.; Landers, R.; Benvenutt, E.V.; Machado, S.A.S. Sol–gel thin-film based mesoporous silica and carbon nanotubes for the determination of dopamine, uric acid and paracetamol in urine. *Talanta* **2013**, *116*, 726–735.
105. Canevari, T.C.; Raymundo-Pereira, P.A.; Landers, R.; Machado, S.A.S. Direct synthesis of Ag nanoparticles incorporated on a mesoporous hybrid material as a sensitive sensor for the simultaneous determination of dihydroxybenzenes. *Eur. J. Inorg. Chem.* **2013**, *2013*, 5746–5754.
106. Li, M.; Bo, X.; Mu, Z.; Zhang, Y.; Guo, L. Electrodeposition of nickel oxide and platinum nanoparticles on electrochemically reduced graphene oxide film as a nonenzymatic glucose sensor. *Sens. Actuators B Chem.* **2014**, *192*, 261–268.
107. Kesavan, S.; Revin, S.B.; John, S.A. Potentiodynamic formation of gold nanoparticles film on glassy carbon electrode using aminophenyl diazonium cations grafted gold nanoparticles: Determination of histamine H_2 receptor antagonist. *Electrochim. Acta* **2014**, *119*, 214–224.
108. Fernandes, D.M.; Vos, J.G.; Freire, C. Europium phosphomolybdate and osmium metallopolymer multi-functional LbL films: Redox and electrocatalytic properties. *J. Colloid Interface Sci.* **2014**, *420*, 127–135.
109. Li, M.; Bo, X.; Zhang, Y.; Han, C.; Guo, L. One-pot ionic liquid-assisted synthesis of highly dispersed PtPd nanoparticles/reduced graphene oxide composites for nonenzymatic glucose detection. *Biosens. Bioelectron.* **2014**, *56*, 223–230.
110. Scavetta, E.; Mazzoni, R.; Mariani, F.; Margutta, R.G.; Bonfiglio, A.; Demelas, M.; Fiorilli, S.; Marzocchi, M.; Fraboni, B. Dopamine amperometric detection at a ferrocene clicked PEDOT:PSS coated electrode. *J. Mater. Chem. B* **2014**, *2*, 2861–2867.
111. Kong, C.; Tang, L.; Zhang, X.; Sun, S.; Yang, S.; Song, X.; Yang, Z. Templating synthesis of hollow CuO polyhedron and its application for nonenzymatic glucose detection. *J. Mater. Chem. A* **2014**, *2*, 7306–7312.

112. Zhang, Q.; Pan, D.; Zhang, H.; Han, H.; Kang, Q. Development of a poly(alizarin red S)/ionic liquid film modified electrode for voltammetric determination of catechol. *Electrochim. Acta* **2014**, *133*, 23–29.
113. Doniach, S.; Sunjic, M. Many-electron singularity in X-ray photoemission and X-ray line spectra from metals. *J. Phys. C* **1970**, *3*, 285–291.
114. Yang, D.; Sacher, E. Carbon 1s X-ray Photoemission Line Shape Analysis of Highly Oriented Pyrolytic Graphite: The Influence of Structural Damage on Peak Asymmetry. *Langmuir* **2006**, *22*, 860–862.
115. Desimoni, E.; Casella, G.I.; Cataldi, T.R.I.; Malitesta, C. A comparison of some asymmetrical line shapes for XPS data analysis. *J. Electron Spectrosc. Relat Phenom.* **1989**, *49*, 247–261.